metals

MDPI

Article

Corrosion Resistance of Different Commercial Zr, Zr/Ti and Zr/Cr(III) Conversion Coatings Deposited on an Al Alloy 3003

Maja Mujdrica Kim [1,2] and Ingrid Milošev [2,3,*]

[1] TRIMO d.o.o., Prijateljeva cesta 12, SI-8210 Trebnje, Slovenia; maja.mujdrica@trimo-group.com
[2] Jožef Stefan Postgraduate School, Jamova cesta 39, SI-1000 Ljubljana, Slovenia
[3] Department of Physical and Organic Chemistry, Jožef Stefan Institute, Jamova cesta 39, SI-1000 Ljubljana, Slovenia
* Correspondence: ingrid.milosev@ijs.si

Abstract

Chromate-free conversion coatings are increasingly investigated as environmentally acceptable alternatives to conventional chromate conversion coatings for corrosion protection of aluminum alloys. In the present study, the electrochemical behaviour and long-term corrosion stability of several commercial conversion coating systems based on trivalent chromium (TCP), zirconium (ZrCC) and zirconium/titanium (Zr/TiCC) were systematically evaluated on AA3003 aluminum alloy and compared to chromate conversion coating (CCC) CR614. Three TCP coatings (ST650, MC1300 and B30002), two ZrCC (MC1700 and MC160/161), and one Zr/TiCC (B2040) were investigated. Coatings were prepared at pre-selected pH and concentration, but at varying conversion times. The protective performance of the coating was then tested across various exposure conditions using potentiodynamic polarization measurements: (i) after 24 h of exposure to air, (ii) after 24 h of immersion in 3.5 wt.% NaCl solution and (iii) simulated acid rain solution, and (iv) after exposure in a salt spray chamber for 500 h. The protective performance strongly depended on both the conversion conditions and the exposure environment. The optimal conversion times ranged between 40 s and 18 min, depending on the coating type. Differences between the investigated systems remained relatively limited when investigated after exposure to air and immersion in the simulated acid rain solution. However, in chloride-containing environments, substantially greater differentiation between the coatings was observed. Among the investigated systems, TCP coatings exhibited the most favourable overall corrosion performance, particularly after prolonged salt spray exposure, where ST650 and B30002 polarization resistance values were approximately 8800 and 5300 kΩ cm^2, respectively, together with corrosion current densities as low as 0.0004 and 0.001 μA cm^{-2}. ZrCC systems MC1700 and MC160/161 also provided significant corrosion protection, achieving polarization resistance values around 2700 and 2400 kΩ cm^2 after 500 h of salt spray exposure, whereas the Zr/TiCC coating B2040 exhibited poorer long-term performance. The results further demonstrated that prolonged salt spray exposure provides considerably more realistic evaluation of long-term coating protectiveness than short-term electrochemical measurements alone. Overall, optimized TCP and ZrCC systems provided corrosion protection under chloride-containing conditions comparable to or superior to the investigated conventional chromate conversion coating CR614 deposited on AA3003 alloy.

Keywords: AA3003 aluminum alloy; chromate-free conversion coatings; trivalent chromium process; zirconium conversion coatings; potentiodynamic polarization; salt spray exposure

Academic Editor: Yanxin Qiao

Received: 3 June 2026
Revised: 27 June 2026
Accepted: 28 June 2026
Published: 2 July 2026

1. Introduction

Aluminium alloys are widely used in modern industry due to their low density, favourable mechanical properties and relatively high corrosion resistance [1–3]. Among them, AA3003, a 3xxx series aluminium alloy with manganese as the principal alloying element [4,5], is particularly attractive because it combines good formability with relatively favourable corrosion resistance and is therefore extensively used in building envelope systems, roofing and facade elements, heat exchangers, storage containers and other industrial applications [4,6–8]. In such applications, long-term corrosion protectiveness under varying environmental conditions is essential. In addition, surface pre-treatments are frequently required to improve the adhesion of subsequently applied coatings or adhesives and to ensure long-term durability of bonded or coated products.

Despite the presence of a naturally formed passive oxide layer, aluminium alloys remain susceptible to localised corrosion, particularly in chloride-containing environments [3]. In the case of AA3003, the corrosion behaviour is additionally influenced by microstructural heterogeneity, especially by the presence, composition and distribution of Mn-, Fe- and Si-containing intermetallic phases [9–13]. These heterogeneities may locally modify electrochemical activity, promote passive film breakdown and consequently influence both corrosion initiation and the formation and protective performance of conversion coatings.

For decades, chromate conversion coatings (CCCs) based on hexavalent chromium (chromate, Cr(VI)) were considered among the most effective corrosion protection systems for aluminium alloys due to their excellent barrier properties and self-healing capability [14,15]. However, the toxicity and carcinogenicity of Cr(VI) compounds have led to increasingly strict environmental and occupational regulations restricting their industrial use [14–16]. In parallel with regulatory pressure, corrosion protection is increasingly recognised not only as a technical requirement, but also as an important aspect of sustainability, since premature degradation of metallic materials leads to increased resource consumption, embodied energy losses and additional environmental burden associated with repair and replacement [17–20].

Recent European regulatory developments, including the Ecodesign for Sustainable Products Regulation (ESPR) [21] and Corporate Sustainability Reporting Directive (CSRD) [22], further emphasise durability, material traceability, lifecycle performance and reduction of hazardous substances throughout industrial value chains. Within this broader sustainability-oriented framework, the development of chromate-free conversion coatings is therefore becoming increasingly important not only from the perspective of regulatory compliance but also with regard to circularity, durability and reduced environmental impact [17,18]. Consequently, improved corrosion protection may contribute to extended service life and reduced lifecycle impacts associated with premature degradation and material replacement [20].

As a consequence, considerable research efforts have been focused on the development of environmentally acceptable alternatives to conventional chromate systems, particularly conversion coatings based on zirconium, titanium and trivalent chromium [14–16,23–25]. These systems differ in terms of coating chemistry, formation mechanism and protective behaviour. In general, the formation of TCP and Zr-based conversion coatings is associated with a local pH increase at the alloy surface caused by cathodic reactions, particularly oxygen reduction occurring preferentially on intermetallic particles [15,26–30]. The resulting local alkalization promotes precipitation of Cr- and/or Zr-containing oxide and hydroxide species, forming thin protective conversion layers [15,26,28]. Previous studies further demonstrated that the protective performance of these systems strongly depends on alloy composition, surface preparation, intermetallic particle distribution and coating homogeneity [15,27,31–36]. Recent investigations have additionally highlighted the important

influence of conversion bath composition, pH and treatment time on coating morphology, composition and corrosion resistance [37]. In addition to TCP and zirconium-based systems, alternative chromium-free approaches based on cerium-containing protective layers have also demonstrated promising corrosion protection and long-term durability on aluminium alloys [38].

Among chromate-free systems, trivalent chromium conversion coatings (TCP) are particularly attractive because they may provide corrosion protection comparable to conventional chromate coatings while avoiding the direct use of Cr(VI) species [15,26,27,32]. TCP coatings are generally composed of mixed Cr- and Zr-containing oxides and hydroxides and often exhibit a multilayer structure consisting of Al/O/F-rich inner regions and Cr/Zr-rich outer regions [15,26,32,39]. Several studies also suggested the possibility of partial self-healing behaviour associated with the mobility of Cr-containing species within the coating [32,39–42]. In contrast, zirconium- and titanium-based conversion coatings (ZrCC and Zr/TiCC) are primarily based on barrier protection provided by thin oxide and hydroxide layers formed through precipitation of Zr- and/or Ti-containing species [14,25]. Their main advantages include low process complexity, low coating thickness, reduced environmental impact and absence of highly toxic chromate compounds [43–46].

Numerous studies have investigated TCP and ZrCC systems on aluminium alloys such as AA2024, AA6061, AA7075 and AA5052 [15,27,32,41,47,48]. However, considerably less information is available for AA3003 alloy, particularly regarding systematic comparison of different commercial conversion coating systems under varying environmental conditions [25,49,50]. Furthermore, most electrochemical evaluations are commonly performed only in a single electrolyte, typically a chloride-containing solution, which does not necessarily reflect the complexity of real service environments.

Previous studies also demonstrated that the exposure environment may significantly influence the electrochemical response and apparent protective performance of conversion coatings [27,32,51,52]. Chloride-containing electrolytes promote localised corrosion processes and therefore represent a highly sensitive environment for differentiation of coating performance, whereas milder environments may be dominated primarily by passive behaviour of the aluminium substrate itself. In addition, stabilisation and structural reorganisation processes may continue after coating deposition, further affecting corrosion response during subsequent exposure [32,51–53].

Therefore, a systematic comparison of different commercial chromate-free conversion coatings under different environmental conditions is necessary to better understand their protective behaviour and limitations on AA3003 alloy. In contrast to most previous studies, which focused on individual coating technologies or a single exposure environment, the present work compares six commercially available chromate-free conversion coating systems representing TCP, ZrCC and Zr/TiCC technologies together with a conventional chromate conversion coating reference. The coatings were evaluated under four different exposure conditions, including air exposure, immersion in chloride-containing electrolyte, and simulated acid rain and prolonged salt spray testing, enabling direct comparison of both short-term electrochemical behaviour and long-term corrosion stability under identical experimental conditions. Particular emphasis was placed on optimisation of conversion conditions and on assessment of the practical corrosion protection performance of commercially relevant coating systems on AA3003 aluminium alloy, providing insight into their relative corrosion protection performance under different environmental conditions and their long-term stability during salt spray exposure. So, the focus of this study is the comparison of the electrochemical performance of six commercial conversion coatings across multiple exposure conditions and their evaluation with respect to CCCs, rather than a detailed structural, chemical and mechanistic validation, which was

already reported in our previous studies for the TCP (ST650 [52] and MC1300 [54]) and ZrCC MC1700 [54] coatings deposited on AA3003 and similar ZrCC coatings on various aluminum alloys [42,51,53,55–57] and steel and Zn substrates [58]. The surface-analytical results obtained in these studies are used to substantiate the electrochemical results.

2. Materials and Methods

2.1. Materials and Sample Preparation

For this study, 50 µm thick aluminium alloy EN AW-3003 H19 foil, produced by Impol d.o.o. (Slovenska Bistrica, Slovenia), was used. The chemical composition of the alloy, as specified by the manufacturer, was Mn 1.1 wt.%, Fe 0.6 wt.%, Si 0.14 wt.%, Cu 0.13 wt.%, Zn 0.009 wt.%, Cd 0.0003 wt.%, and Al 98.1 wt.%. The foil was cut into specimens with dimensions of 20 mm × 40 mm.

The samples were initially ultrasonically cleaned in absolute ethanol (99.0%, Carlo Erba Reactants, Rodano, Italy) for 3 min using an ultrasonic bath (Elmasonic P 30 H, Elma Schmidbauer GmbH, Singen, Germany) to remove surface impurities and subsequently dried in a stream of compressed nitrogen. These samples are hereafter denoted as AA3003. The average surface roughness (R_a) of the untreated AA3003 substrate was 0.175 ± 0.0051 µm. The measurements were performed using a stylus contact profilometer, Bruker DektakXT (Bruker, Billerica, MA, USA) equipped with a 2 µm tip operating in soft-touch mode with a force of 1 mN. Five randomly selected 4 mm long lines were analysed. The collected data were processed using TalyMap Gold 6.2 software.

Mechanical grinding was not performed prior to conversion treatment. Preliminary experiments showed that mechanical abrasion caused surface cracking due to the low thickness (50 µm) of the aluminium alloy foil, making such treatment unsuitable.

The following chemicals were used for chemical surface pre-treatment: SurTec® 132 and SurTec® 089 cleaning agents (SurTec International GmbH, Bensheim, Germany) and nitric acid (65%, Sigma-Aldrich, Saint Louis, MO, USA). The major component of the slightly alkaline cleaner SurTec® 132 is tetrapotassium pyrophosphate. The cleaner is free of silicates and surfactants and has a pH of 8.3. SurTec® 089 contains non-ionic surfactants such as amines, coco alkyl compounds and ethoxylated fatty alcohols.

Milli-Q Direct water with resistivity ≥ 18 MΩ cm at 25 °C (Millipore, Billerica, MA, USA) was used for rinsing and preparing all solutions.

Prior to the deposition of conversion coatings, the aluminium surface was chemically pre-treated using a combined alkaline and acidic cleaning procedure, denoted as CP-AA3003 (Figure 1a). The optimisation of the surface pre-treatment procedure was reported in our previous study [52]. Based on these results, the final pre-treatment process consisted of alkaline cleaning in a mixture of 2 wt.% SurTec® 132 and 0.5 wt.% SurTec® 089 at 40 °C for 3 min, followed by desmutting for 30 s at room temperature in 50 vol.% HNO_3 solution. After chemical pre-treatment and desmutting, the samples were rinsed with Milli-Q Direct water and dried in a stream of compressed nitrogen. The optimised procedure was subsequently used for all samples prior to conversion coating deposition.

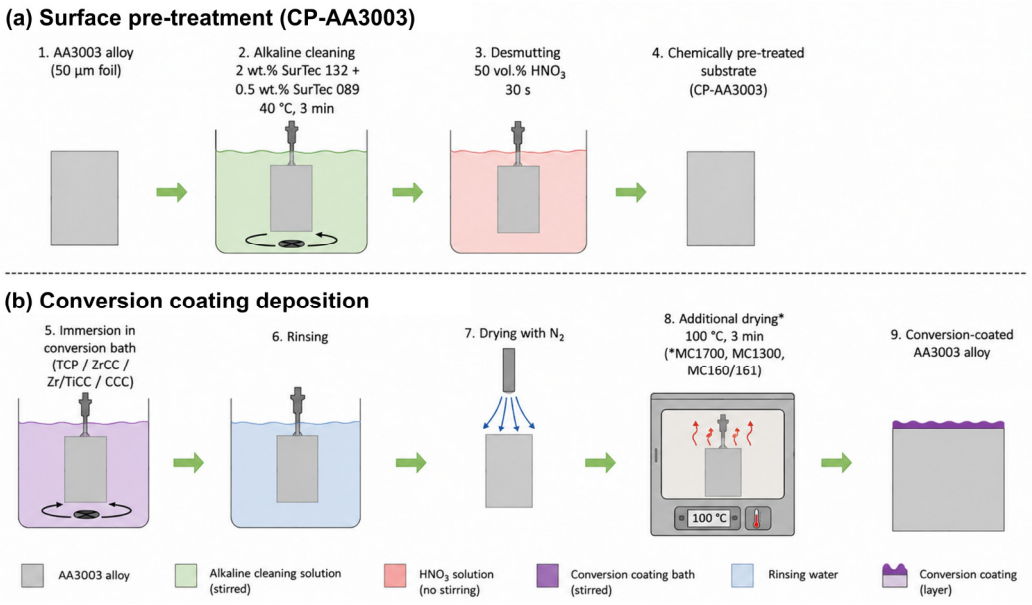

Figure 1. Schematic illustration of the chemical pre-treatment and conversion coating deposition procedure for AA3003 alloy.

The composition, trade names, coating types and manufacturers of commercially available conversion coatings used in this study are summarised in Table 1, along with their abbreviations. The investigated systems comprised trivalent chromium process (TCP) coatings, including ST650, MC1300 and B30002, zirconium-based conversion coatings (ZrCC), including MC1700 and MC160/161, zirconium/titanium-based conversion coating (Zr/TiCC), and conventional chromate conversion coating (CCC) CR614.

Table 1. Commercial conversion coating systems investigated in this study.

Trade Name	Abbreviation	Composition	Coating Type	Manufacturer
SurTec® 650	ST650	H_2ZrF_6 + Cr(III)	TCP	SurTec International GmbH, Bensheim, Germany
MAVOMcoat 1700	MC1700	H_2ZrF_6	ZrCC	MAVOM Chemie BV, Alphen aan den Rijn, The Netherlands
MAVOMcoat 1300	MC1300	H_2ZrF_6 + Cr(III)	TCP	MAVOM Chemie BV, Alphen aan den Rijn, The Netherlands
MAVOMcoat 160/161	MC160/161	H_2ZrF_6	ZrCC	MAVOM Chemie BV, Alphen aan den Rijn, The Netherlands
Bonderite® M-NT 2040	B2040	H_2TiF_6 + H_2ZrF_6	Zr/TiCC	Henkel AG & Co. KGaA, Düsseldorf, Germany
Bonderite® M-NT 30002	B30002	H_2ZrF_6 + Cr(III)	TCP	Henkel AG & Co. KGaA, Düsseldorf, Germany
Cromcoat CR 614	CR614	Cr(VI)-based chromating system	CCC	Condoroil Chemical S.r.l., Casale Litta, Italy

Electrochemical measurements were performed in two different electrolytes: (i) 3.5 wt.% NaCl solution (99.7%, Fisher Scientific, Hampton, NH, USA), pH ≈ 5.5, and (ii) simulated acid rain consisting of 0.2 g Na_2SO_4 (99%, Acros Organics, Hampton, NH, USA), 0.2 g $NaHCO_3$ (Sigma-Aldrich, Saint Louis, MO, USA), and 0.2 g $NaNO_3$ (99%, Sigma-Aldrich, Saint Louis, MO, USA) dissolved in 1 L of water. The pH of the solution ika stirrer manufacturerika stirrerlona, Spain).

2.2. Conversion Coating Deposition and Processing

All conversion coatings were deposited on chemically pre-treated samples as described above, following the procedure schematically illustrated in Figure 1b. The coatings were prepared by immersion of the samples in the working conversion bath contained in a 250 mL polyethylene vessel. The bath was continuously stirred using a magnetic stirrer at 250 rpm (IKA C-MAG HS7, IKA-Werke GmbH & Co K, Staufen, Germany). After deposition, the samples were rinsed with 50 mL of Milli-Q water, immersed in fresh Milli-Q water for 1 min at room temperature, and finally dried in a stream of compressed nitrogen. Additional drying at 100 °C for 3 min was performed for MC1700, MC1300 and MC160/161 coatings (Table 2).

Table 2. Deposition parameters used for the preparation of the investigated conversion coatings.

Coating	Concentration	Target pH	Actual pH	pH Adjustment Additive	T_{conv}	t_{conv}	Additional Treatment
ST650	10 vol.%	3.7–3.95	3.9	1% NaOH or 5% H_2SO_4	RT	90 s, 11 min, 18 min	-
MC1700	5 wt.%	3.8–5.5	4.4	15% NH_4HCO_3	RT	120 s, 10 min, 18 min, 30 min	Drying for 3 min at 100 °C
MC1300	5 wt.%	3.5–4.5	4.1	25% NH_3(aq)	RT	80 s, 7 min, 18 min, 45 min	Drying for 3 min at 100 °C
MC160/161	1 wt.% MC160 1 wt.% MC161	n.a.	n.a.	-	RT	40 s, 10 min, 18 min, 45 min	Drying for 3 min at 100 °C
B2040	1.4 wt.%	n.a.	1.1	-	40 °C	80 s, 10 min, 18 min, 50 min	-
B30002	3 wt.%	4–4.5	4.3	15% NH_4HCO_3 or HNO_3	RT	80 s, 13 min, 18 min	-
CR614	1.5 wt.%	n.a.	-	-	35 °C	3 min	-

The selection of bath concentration, pH and recommended temperature range was based on manufacturers' technical data sheets and recommendations [59–65]. In most cases, the conversion treatments were carried out at room temperature (RT), even when elevated temperatures were recommended by the manufacturer, in order to evaluate the applicability of the systems under lower-energy industrial processing conditions.

The conversion time (t_{conv}) was selected based on the manufacturers' recommendations and preliminary OCP measurements performed during coating deposition. The investigated deposition parameters for individual conversion coating systems are summarized in Table 2.

2.3. Electrochemical Measurements

Prior to potentiodynamic polarisation (PD) measurements, separate sets of coated samples were immediately subjected to one of the following post-treatment conditions after coating preparation and drying:

(i) Exposure to air for 24 h.

(ii) Immersion in 3.5 wt.% NaCl solution for 24 h.

(iii) Immersion in simulated acid rain for 24 h.

(iv) Exposure in a salt spray chamber for 500 h.

Electrochemical measurements were carried out at room temperature in a conventional three-electrode corrosion cell (K0235 Flat Cell Kit, volume 250 mL, Metrohm Autolab, Utrecht, The Netherlands) made of a glass cylinder and Teflon side walls. The specimen (working electrode) was positioned vertically at the Teflon side wall and pressed against a Teflon ring to expose an area of 1 cm^2. An Ag/AgCl electrode saturated with AgCl/KCl (0.197 V vs. standard hydrogen electrode) was used as the reference electrode, while a platinum mesh served as the counter electrode. The Ag/AgCl reference electrode was immersed vertically into the electrolyte and positioned close to the working electrode surface. Electrochemical experiments were performed using a potentiostat/galvanostat Autolab PGSTAT 12 (Metrohm Autolab, Utrecht, The Netherlands) controlled by Nova 2.1 software. All potentials reported in this work are referred to the Ag/AgCl scale. Before each measurement, the electrode was stabilised at open circuit potential (OCP) for 1 h to attain a quasi-steady-state condition. According to the criterion proposed by Kelly [66], the OCP was considered stabilised when the potential variation during 10 min was less than 5 mV. Linear polarisation measurements were subsequently performed in the range of ±10 mV vs. OCP using a scan rate (dE/dt) of 0.1 mV/s. The polarisation resistance (R_p) was determined from the slope of the current density vs. potential dependence using Nova software. Potentiodynamic polarisation measurements were then carried out at a scan rate of 1 mV/s starting from −250 mV vs. OCP in the anodic direction until the current reached 0.1 mA.

Each measurement was repeated at least three times at different locations on the same coated specimen. The electrochemical parameters reported in the tables are presented as mean ± standard deviation values. The reported standard deviations, therefore, reflect the variability of the electrochemical response across the coated surface. The reproducibility between independently prepared coating batches was not investigated in the present study.

Electrochemical corrosion parameters, including corrosion potential (E_{corr}), corrosion current density (j_{corr}), and breakdown potential (E_{bd}) were determined from polarisation curves using the Tafel approximation in Nova 2.1 software. The breakdown potential was defined as the potential at which the current density abruptly increased within the passive region. The passive range was expressed as $\Delta E = |E_{bd} - E_{corr}|$. In cases where no clearly defined anodic Tafel region was observed, the corrosion current density was estimated from the cathodic branch extrapolation intersecting the line corresponding to E_{corr}. In such cases, the obtained j_{corr} values should be regarded as approximate estimates and interpreted together with the polarisation resistance and overall polarisation behaviour.

2.4. Salt Spray Test

Salt spray tests were performed according to the ISO 9227:2017 standard (corrosion tests in artificial atmospheres—salt spray tests) [67] using a chamber with a volume of 0.17 m^3 (ASCOTT, Staffs, UK).

A 5 wt.% NaCl solution prepared with Milli-Q water was used as the testing electrolyte and filtered prior to use. The test was carried out at a spray pressure of 85 kPa and a solution flow rate of 5–10 mL/min. The temperature of the humidifying chamber was maintained at 46 °C, while the chamber temperature was 35 ± 2 °C.

Prior to testing, the sample edges were protected with adhesive tape to prevent corrosion of uncoated areas. The samples were positioned in a plastic holder at an angle of approximately 45° from the vertical direction.

The total exposure time was 500 h. Corrosion progression was monitored visually and documented photographically at selected time intervals when surface changes were observed.

After completion of the salt spray exposure, the samples were rinsed with Milli-Q water and dried under nitrogen prior to potentiodynamic measurements.

3. Results and Discussion

The corrosion protection performance of the investigated conversion coating systems on AA3003 alloy was evaluated under different post-treatments and exposure conditions. The comparative analysis included TCP, ZrCC, Zr/TiCC and CCC conversion coatings. For each conversion coating system, only samples exhibiting the best protective performance were included in the comparative analysis. Electrochemical data after 24 h exposure to air were not available for ST650; therefore, this coating was not included in the air-exposure comparison. The optimal conversion times (t_{conv}) used in the comparative discussion were selected based on high R_p and low j_{corr}, while ΔE was used as an additional criterion when the first two parameters did not allow clear identification of the optimal conditions. The complete optimisation results, including electrochemical parameters obtained at different deposition conditions, are provided in Appendix A.

The electrochemical behaviour of the selected conversion coatings was evaluated for various post-treatments: after 24 h exposure to air, immersion in 3.5 wt.% NaCl solution, and immersion in simulated acid rain, and after prolonged exposure in a salt spray chamber for 500 h.

3.1. Effect of Post-Treatment Environment on Corrosion Response

The electrochemical behaviour of the investigated conversion coatings strongly depended on both the post-treatment condition and the exposure environment. Figure 2 presents representative potentiodynamic polarisation curves corresponding to the optimal conversion time selected for each coating system based on the highest polarisation resistance and lowest corrosion current density obtained after 24 h exposure in air, 3.5 wt.% NaCl solution and simulated acid rain solution. The corresponding electrochemical parameters and optimal conversion times are summarised in Tables 3–5. Detailed potentiodynamic polarisation curves and electrochemical parameters obtained for all investigated conversion times are provided in Appendix A (Figures A1–A6 and Tables A1–A6). The results demonstrated that post-treatment conditions strongly influence the electrochemical response of the investigated systems. Differences between coatings were relatively limited after air exposure, whereas substantially greater differentiation in polarisation resistance (R_p) and overall polarisation behaviour was observed after exposure to a chloride-containing electrolyte. In simulated acid rain, the electrochemical responses of the investigated systems became more similar, particularly in terms of R_p and j_{corr} values, due to the lower aggressiveness of the electrolyte.

Table 3. Electrochemical parameters of conversion coatings on CP-AA3003 after 24 h exposure to air. The polarisation resistance (R_p) was determined from the linear polarisation measurements, and the corrosion potential (E_{corr}), corrosion current density (j_{corr}), breakdown potential (E_{bd}) and $\Delta E = |E_{bd} - E_{corr}|$ from potentiodynamic polarisation curves (Figure 2a). Values are given as mean ± standard deviation.

Sample	Optimal t_{conv}	R_p (kΩ cm^2)	E_{corr} (V)	j_{corr} (μA cm^{-2})	E_{bd} (V)	ΔE (V)
CP-AA3003	-	1300 ± 200	−0.80 ± 0.01	0.02 ± 0.01	−0.68 ± 0.01	0.12
MC1300	7 min	190 ± 40	−0.72 ± 0.04	0.13 ± 0.11	−0.68 ± 0.02	0.04

Table 3. *Cont.*

Sample	Optimal t_{conv}	R_p (kΩ cm^2)	E_{corr} (V)	j_{corr} (μA cm^{-2})	E_{bd} (V)	ΔE (V)
MC1700	10 min	530 ± 60	−1.01 ± 0.01	0.08 ± 0.01	−0.59 ± 0.02	0.42
B2040	80 s	14 ± 10	−0.71 ± 0.04	1 ± 2	−0.72 ± 0.04	0.01
B30002	80 s	610 ± 90	−0.61 ± 0.02	0.09 ± 0.02	−0.50 ± 0.04	0.11
MC160/161	40 s	226 ± 81	−0.92 ± 0.11	0.21 ± 0.06	−0.64 ± 0.03	0.29
CR614	3 min	521 ± 139	−0.72 ± 0.01	0.03 ± 0.001	−0.52 ± 0.03	0.20

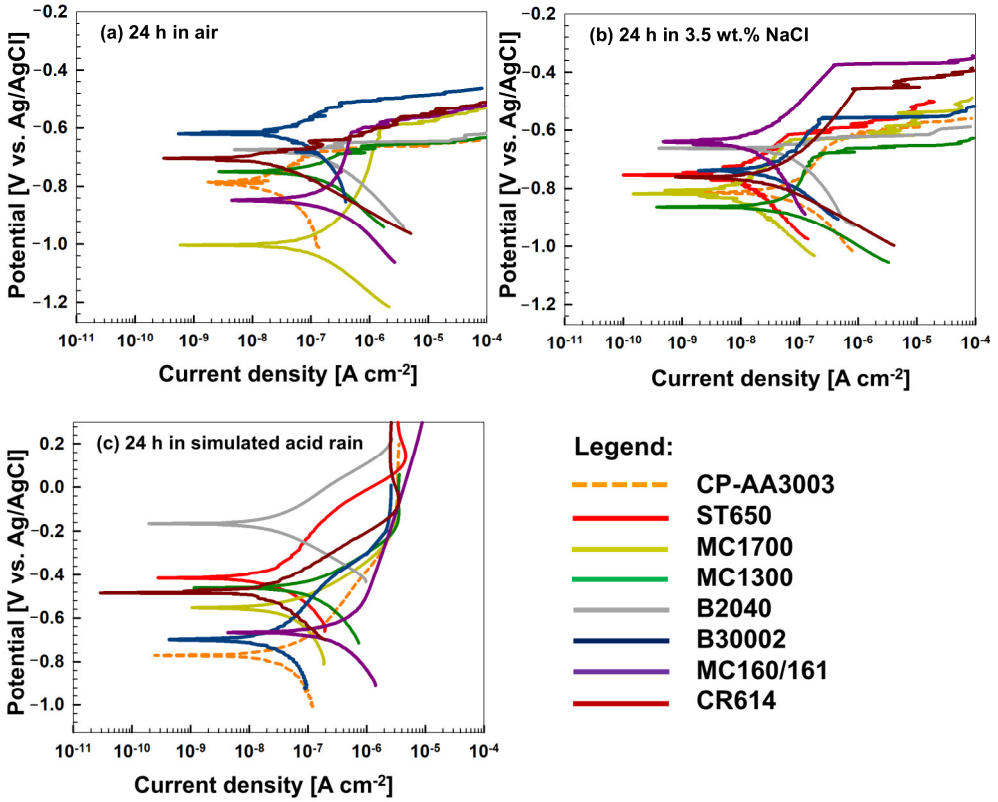

Figure 2. Comparative potentiodynamic polarisation curves of conversion coatings on CP-AA3003 after 24 h post-treatment exposure under different conditions: (**a**) air, (**b**) 3.5 wt.% NaCl solution, and (**c**) simulated acid rain. Electrochemical measurements were performed in 3.5 wt.% NaCl for (**a**,**b**) and in simulated acid rain solution for (**c**). Scan rate: dE/dt = 1 mV/s. The optimal conversion times for each conversion coating and corresponding electrochemical parameters are summarised in Tables 3–5. All potentials (E) are given versus the Ag/AgCl reference electrode.

Table 4. Electrochemical parameters of conversion coatings on CP-AA3003 after 24 h exposure to 3.5 wt.% NaCl solution. The polarisation resistance (R_p) was determined from the linear polarisation measurements, and the corrosion potential (E_{corr}), corrosion current density (j_{corr}), breakdown potential (E_{bd}) and $\Delta E = |E_{bd} - E_{corr}|$ from potentiodynamic polarisation curves (Figure 2b). Values are given as mean ± standard deviation.

Sample	Optimal t_{conv}	R_p (kΩ cm^2)	E_{corr} (V)	j_{corr} (μA cm^{-2})	E_{bd} (V)	ΔE (V)
CP-AA3003	-	740 ± 50	−0.80 ± 0.02	0.06 ± 0.03	−0.64 ± 0.02	0.17
ST650	18 min	1927 ± 73	−0.76 ± 0.01	0.01 ± 0.01	−0.59 ± 0.04	0.17
MC1300	7 min	890 ± 70	−0.86 ± 0.01	0.05 ± 0.01	−0.67 ± 0.01	0.18

Table 4. *Cont.*

Sample	Optimal t_{conv}	R_p (kΩ cm^2)	E_{corr} (V)	j_{corr} (μA cm^{-2})	E_{bd} (V)	ΔE (V)
MC1700	10 min	2000 ± 500	−0.80 ± 0.02	0.01 ± 0.03	−0.63 ± 0.01	0.17
B2040	80 s	50 ± 30	−0.67 ± 0.01	0.10 ± 0.06	−0.63 ± 0.01	0.03
B30002	80 s	840 ± 10	−0.76 ± 0.02	0.01 ± 0.07	−0.54 ± 0.01	-
MC160/161	40 s	1500 ± 537	−0.63 ± 0.03	0.03 ± 0.02	−0.38 ± 0.01	0.25
CR614	3 min	993 ± 13	−0.74 ± 0.03	0.03 ± 0.01	−0.52 ± 0.08	0.15

Table 5. Electrochemical parameters of conversion coatings on CP-AA3003 after 24 h exposure to simulated acid rain. The polarisation resistance (R_p) was determined from the linear polarisation measurements, and the corrosion potential (E_{corr}), corrosion current density (j_{corr}), breakdown potential (E_{bd}) and $\Delta E = |E_{bd} - E_{corr}|$ from potentiodynamic polarisation curves (Figure 2c). Values are given as mean ± standard deviation.

Sample	Optimal t_{conv}	R_p (kΩ cm^2)	E_{corr} (V)	j_{corr} (μA cm^{-2})
CP-AA3003	-	830 ± 230	−0.76 ± 0.01	0.06 ± 0.03
ST650	18 min	1545 ± 716	−0.66 ± 0.22	0.03 ± 0.02
MC1300	80 s	520 ± 260	−0.58 ± 0.16	0.08 ± 0.01
MC1700	120 s	1200 ± 320	−0.59 ± 0.05	0.05 ± 0.02
B2040	18 min	990 ± 570	−0.16 ± 0.01	0.03 ± 0.01
B30002	80 s	880 ± 110	−0.79 ± 0.14	0.06 ± 0.05
MC160/161	18 min	286 ± 196	−0.46 ± 0.18	0.11 ± 0.16
CR614	3 min	517 ± 231	−0.43 ± 0.07	0.03 ± 0.01

The optimal conversion times differed between the investigated coating systems and exposure conditions, indicating that the protective performance of the conversion coatings is strongly influenced by the conversion process itself. In general, conversion time affects coating growth, surface coverage and homogeneity, which consequently influence the electrochemical stability and barrier properties of the formed conversion layer [15,52]. Insufficient conversion time may lead to incomplete coating formation and limited protection, whereas excessively prolonged conversion treatment may promote increased surface heterogeneity, crack formation or substrate dissolution, particularly in highly acidic conversion baths, as reported previously for similar conversion coating systems [15,52]. Consequently, the optimal conversion conditions represent a balance between sufficient coating formation and preservation of electrochemical stability. The detailed influence of conversion time on the electrochemical response of individual coating systems is presented in Figures A1–A6 and Tables A1–A6.

After 24 h exposure in air, the differences between individual coating systems were relatively small (Figure 2a, Table 3). The chemically pre-treated reference sample (CP-AA3003) exhibited the highest polarisation resistance (1300 kΩ cm^2) together with the lowest corrosion current density (0.02 μA cm^{-2}), indicating that under low-aggressiveness conditions the electrochemical response is dominated primarily by the naturally formed passive aluminium oxide layer on the substrate surface [52,54]. Consequently, the protective contribution of thin conversion coatings remains relatively limited after simple air exposure, resulting in only minor differences between the investigated systems. Among the investigated conversion coatings, B30002 (TCP), MC1700 (ZrCC), and CR614 (CCC) showed the highest R_p values, ranging between approximately 500 and 600 kΩ cm^2. The CCC exhibited the lowest j_{corr} value among coated samples, while MC1700 showed the largest ΔE value (0.42 V), indicating improved resistance to localised corrosion. In contrast, MC1300

and MC160/161 exhibited lower R_p values and higher j_{corr}, whereas B2040 showed the poorest electrochemical response, characterised by very low R_p and high j_{corr} values. The poor behaviour of B2040 is associated with the highly acidic conversion bath (pH ≈ 1.14), which promotes intensive dissolution of the aluminium substrate during coating formation. Under such conditions, dissolution of the native oxide layer and substrate surface likely proceeds faster than precipitation of stable Zr- and Ti-containing species, which may hinder the formation of a compact and continuous conversion layer. As a result, the coating may provide only limited barrier protection.

After 24 h exposure in 3.5 wt.% NaCl solution, substantially greater differentiation in R_p values and polarisation curve characteristics was observed among the investigated systems. (Figure 2b, Table 4). In contrast to air exposure, most conversion coatings exhibited improved corrosion resistance compared to the chemically pre-treated reference sample CP-AA3003, confirming their protective effect in a chloride-containing environment. The greater spread of R_p values indicates that the NaCl environment provides a significantly more demanding and more sensitive test for evaluation of thin conversion coatings than simple air exposure or simulated acid rain. Chloride ions are known to locally destabilise the passive aluminium oxide layer and promote localised corrosion processes [68,69]. In aluminium alloys containing Fe- and Mn-rich intermetallic particles, chloride-induced attack frequently initiates at or around these heterogeneities due to local galvanic interactions and passive film breakdown [70]. Consequently, even relatively small differences in coating compactness, defect density and electrochemical stability become more clearly expressed in NaCl solution. The highest polarisation resistance values were obtained for MC1700 (ZrCC) and ST650 (TCP), reaching approximately 2000 and 1900 kΩ cm^2, respectively, while both coatings simultaneously exhibited the lowest corrosion current density (0.01 μA cm^{-2}). The improved behaviour of ST650 is associated with suppression of both anodic and cathodic reactions, as reflected by the lower current densities over the entire polarisation range. The reduction in anodic currents can be attributed to passivation of the aluminium matrix surrounding intermetallic particles [15,52], whereas the lower cathodic currents indicate hindered oxygen reduction due to the barrier effect of the conversion layer. A similarly favourable response was observed for MC1700, which exhibited the highest R_p value together with a relatively broad passive region. Previous surface and EDS analyses reported in our earlier work [54] showed that the optimised MC1700 coating forms a relatively homogeneous Zr-rich conversion layer. After 24 h immersion in NaCl solution, the coating exhibited increased oxygen content together with reduced fluorine concentration compared to samples exposed only to air, which may be associated with a gradual transformation of fluoride-containing species into a more stable oxide/hydroxide-rich surface layer, as reported previously for similar zirconium-based conversion coatings [51,52,54–56]. Previous studies have further associated such behaviour with densification and self-sealing processes occurring in zirconium-based conversion coatings exposed to chloride-containing environments [51,52,54–56]. These processes may contribute to improved electrochemical stability and enhanced resistance to localised corrosion after prolonged immersion in NaCl solution.

The MC160/161 coating also exhibited relatively high R_p values and the highest ΔE value among all investigated systems, indicating improved resistance to localised corrosion. In contrast, MC1300 and B30002 showed only moderate improvement compared to CP-AA3003, while B2040 again exhibited the poorest electrochemical behaviour, characterised by low R_p and relatively high j_{corr} values. This behaviour is consistent with the limited stability and poor barrier properties of the B2040 conversion layer discussed above. Consequently, prolonged conversion times lead predominantly to increased electrochemical activity rather than improved barrier protection (Figure A4, Table A4).

The results further demonstrate that the chloride-containing environment more effectively differentiates the protective performance of thin conversion coatings than air exposure or simulated acid rain. Similar observations were previously reported for TCP coatings on AA2024 and ZrCC coatings on AA5754 [58,71]. In addition, our previous study on MC1700 and MC1300 coatings [54] showed that electrochemical measurements immediately after preparation do not necessarily reflect the real protective performance of thin conversion coatings, since stabilisation and maturation processes continue after coating deposition.

In simulated acid rain, the differences between the investigated conversion coatings were less pronounced than in the chloride-containing electrolyte, particularly with respect to R_p and j_{corr} values (Figure 2c, Table 5), which is attributed to the lower aggressiveness of the electrolyte and the absence of chloride-induced localised corrosion. In this environment, corrosion processes are governed predominantly by the general passive behaviour of the aluminium surface rather than by chloride-induced localised breakdown of the oxide layer [68]. Consequently, subtle differences in protective performance between individual conversion coatings become considerably less pronounced than in a chloride-containing solution. Under these conditions, the chemically pre-treated substrate CP-AA3003 already exhibited relatively favourable electrochemical behaviour, with R_p around 830 kΩ cm^2 and j_{corr} of 0.06 μA cm^{-2}.

Among the investigated systems, ST650 (TCP) and MC1700 (ZrCC) again exhibited the most favourable electrochemical response, reaching R_p values of approximately 1500 and 1200 kΩ cm^2, respectively. ST650 additionally showed reduced j_{corr} values (0.03 μA cm^{-2}), indicating improved electrochemical stability also in a less aggressive environment. The favourable behaviour of MC1700 is consistent with the optimised Zr-rich conversion layer reported previously in our study [54]. The B2040 coating exhibited improved electrochemical parameters in simulated acid rain compared to chloride-containing electrolyte, particularly at longer conversion times (Figure A4c, Table A4). However, the improved behaviour is mainly associated with the lower aggressiveness of the electrolyte rather than with the formation of a robust protective barrier. At the same time, somewhat lower reproducibility of the measurements was observed for longer conversion times, which may indicate the formation of less homogeneous conversion layers. In contrast, MC1300 and B30002 exhibited electrochemical parameters comparable to CP-AA3003, indicating only a limited additional protective effect in simulated acid rain. The poorest behaviour was observed for MC160/161, which showed the lowest R_p and highest j_{corr} values among the investigated systems. Interestingly, the conventional chromate conversion coating CR614 also did not exhibit significantly superior electrochemical behaviour in this environment, as its electrochemical parameters remained comparable to several chromate-free systems. Overall, the results indicate that simulated acid rain provides less differentiation between the investigated conversion coatings in terms of R_p and j_{corr} values than the chloride-containing electrolyte. The dominant electrochemical response in this medium is associated with passive behaviour of the aluminium substrate itself, while the contribution of the conversion coatings to additional barrier protection remains limited.

For a more comprehensive comparison of the protective performance of the investigated conversion coatings in different environments, the corresponding R_p and j_{corr} values are summarised in Figure 3. The coatings are comparatively ranked according to their R_p values obtained in each environment, enabling direct comparison of their relative corrosion resistance. The results confirm that the electrochemical response strongly depends on the exposure medium. Among the investigated systems, ST650 (TCP) and MC1700 (ZrCC) exhibited the most stable and favourable behaviour across all tested conditions, while MC160/161 (ZrCC) and CR614 (CCC) showed good performance mainly in NaCl solution.

B30002 and MC1300 displayed intermediate behaviour, whereas B2040 (Zr/TiCC) exhibited the least favourable electrochemical response under the investigated conditions.

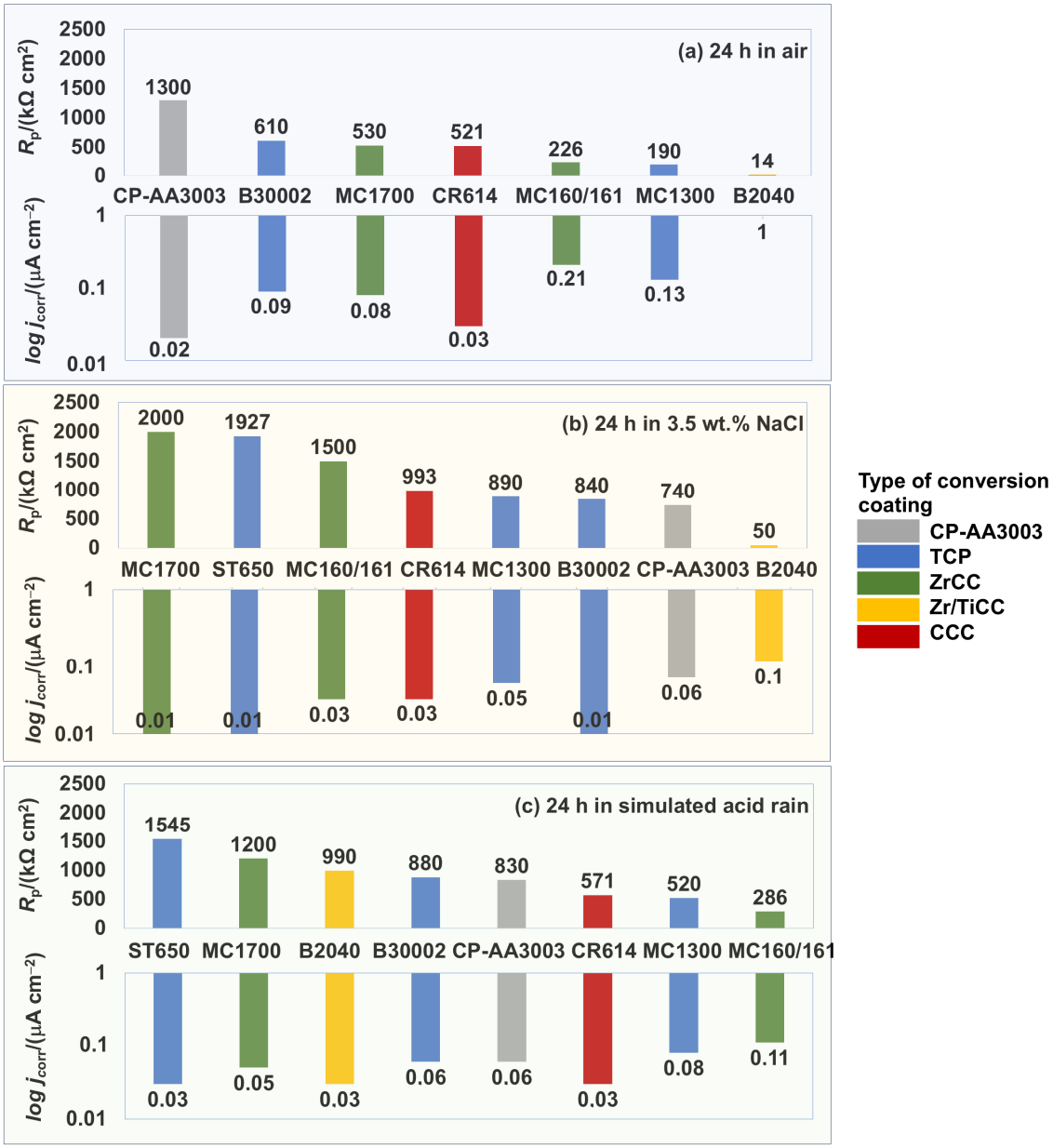

Figure 3. Comparative presentation of polarisation resistance (R_p) and corrosion current density (j_{corr}) of conversion coatings on CP-AA3003 after 24 h post-treatment in different environments: (**a**) air, (**b**) 3.5 wt.% NaCl, and (**c**) simulated acid rain. The j_{corr} values are presented on a logarithmic scale.

Finally, it should be noted that the optimal conversion times vary depending on the coating type and exposure conditions (Tables 3–6 and A1–A7). In general, ST650 and MC1700 require longer optimal conversion times but provide superior performance. MC1300 also requires a relatively long conversion time. In contrast, the optimal conversion times for B3003 and B2040 are considerably shorter; however, their performance is also less favourable. Moreover, longer conversion times are generally required to withstand the harsher conditions associated with prolonged exposure in a salt spray chamber. Therefore, the best protective properties are not necessarily achieved with the shortest preparation times. In many cases, longer conversion times are required to obtain the desired level of protection.

Table 6. Electrochemical parameters of conversion coatings on CP-AA3003 and conversion-coated samples after 500 h exposure in a salt spray chamber. The polarisation resistance (R_p) was determined from the linear polarisation measurements, and the corrosion potential (E_{corr}), corrosion current density (j_{corr}), breakdown potential (E_{bd}) and $\Delta E = |E_{bd} - E_{corr}|$ from potentiodynamic polarisation curves (Figure 4). Values are given as mean ± standard deviation.

Sample	Optimal t_{conv}	R_p (kΩ cm^2)	E_{corr} (V)	j_{corr} (μA cm^{-2})	E_{bd} (V)	ΔE (V)
CP-AA3003	-	36 ± 3	−0.71 ± 0.01	1.0 ± 0.4	−0.59 ± 0.01	0.13
ST650	11 min	8800 ± 1700	−0.64 ± 0.20	0.0004 ± 0.001	−0.24 ± 0.02	0.39
MC1300	18 min	1500 ± 1500	−0.68 ± 0.06	0.06 ± 0.02	−0.60 ± 0.002	0.08
MC1700	10 min	2700 ± 50	−0.72 ± 0.01	0.004 ± 0.002	−0.44 ± 0.05	0.28
B2040	80 s	430 ± 80	−0.67 ± 0.03	0.04 ± 0.01	−0.33 ± 0.02	0.35
B30002	18 min	5300 ± 3100	−0.83 ± 0.20	0.001 ± 0.001	−0.44 ± 0.07	0.39
MC160/161	18 min	2424 ± 789	−0.69 ± 0.01	0.005 ± 0.004	−0.21 ± 0.01	0.33
CR614	3 min	116 ± 47	−0.59 ± 0.01	0.20 ± 0.14	−0.08 ± 0.05	0.51

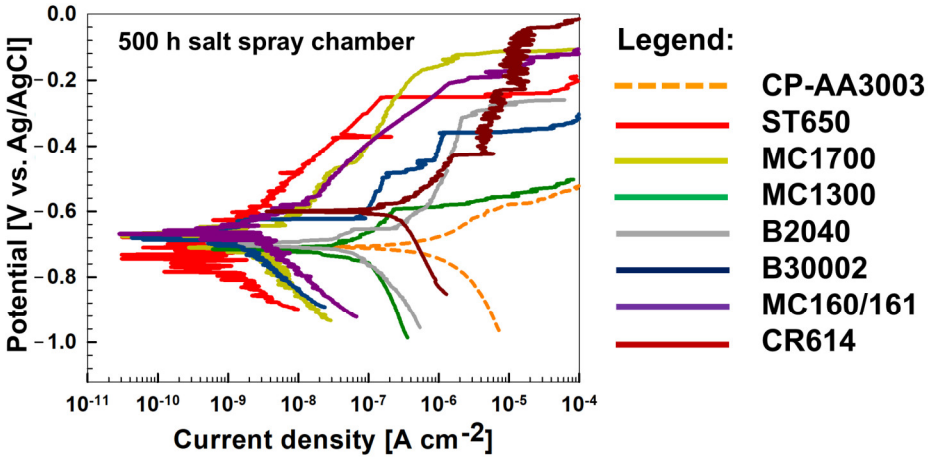

Figure 4. Comparative potentiodynamic polarisation curves of CP-AA3003 and conversion-coated samples after 500 h exposure in a salt spray chamber. The scan rate was dE/dt = 1 mV/s. The optimal conversion time for each conversion coating, and electrochemical parameters deduced from the curves are presented in Table 6.

3.2. Corrosion Behaviour After Prolonged Salt Spray Exposure

The long-term corrosion protectiveness of the investigated conversion coatings was evaluated after 500 h of exposure in a salt spray chamber. Representative potentiodynamic polarisation curves corresponding to the conversion conditions exhibiting the highest polarisation resistance and lowest corrosion current density for each coating system are presented in Figure 4, while the corresponding electrochemical parameters are summarised in Table 6. Detailed potentiodynamic polarisation curves and electrochemical parameters obtained for all investigated conversion times are provided in Appendix A (Figure A7 and Table A7). The results reveal substantially larger differences between the investigated systems after prolonged chloride exposure than after short-term exposure conditions, demonstrating that long-term corrosion stability strongly depends on both coating chemistry and conversion conditions. The relatively large standard deviations observed for some samples after prolonged salt spray exposure likely reflect the heterogeneous nature of localised corrosion processes and increasing surface degradation, which contribute to greater variability in the electrochemical response. Nevertheless, the overall performance trends remained consistent and were supported by multiple electrochemical parameters.

After 500 h exposure, the chemically pre-treated reference sample CP-AA3003 exhibited pronounced electrochemical degradation, characterised by very low polarisation

resistance (36 kΩ cm^2) and high corrosion current density (1.0 µA cm^{-2}) (Figure 4, Table 6). Visual inspection additionally revealed progressive surface degradation during exposure (Figure 5), confirming the limited long-term corrosion resistance of the chemically pre-treated substrate in a chloride-containing environment.

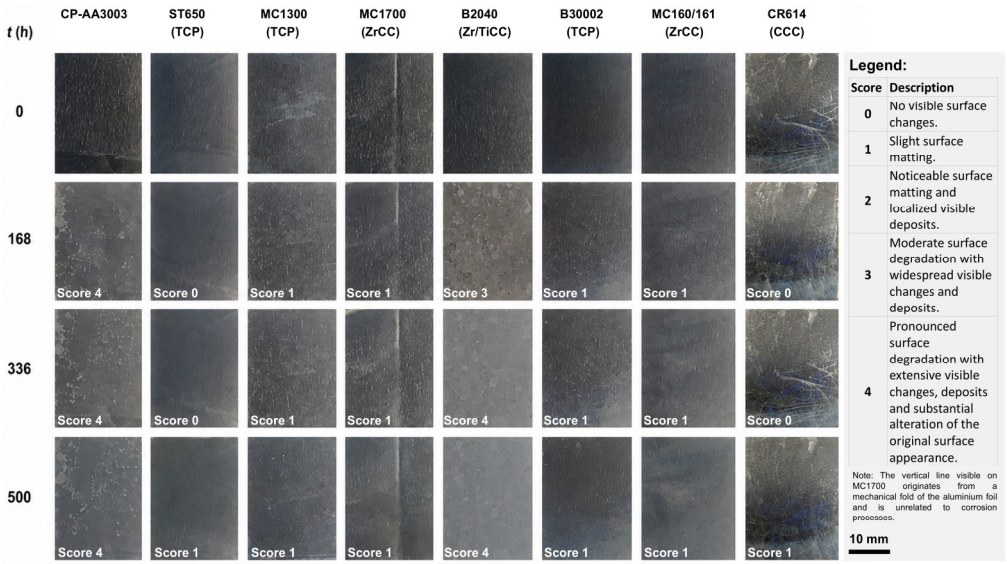

Figure 5. Visual appearance of CP-AA3003 and selected conversion-coated samples during salt spray exposure for up to 500 h. Only coatings exhibiting the most favourable electrochemical performance after 500 h exposure, based on R_p and j_{corr} values obtained from potentiodynamic polarisation measurements (Table 6), are presented.

Among the investigated chromate-free systems, the TCP coatings ST650, MC1300 and B30002 exhibited distinctly different long-term behaviour after salt spray exposure. ST650 and B30002 showed the most favourable electrochemical response, reaching R_p values around 8800 and 5300 kΩ cm^2, together with very low corrosion current densities of 0.0004 and 0.001 µA cm^{-2}, respectively (Table 6, Figure 6). Both coatings also maintained a relatively non-degraded surface appearance during prolonged exposure without pronounced localised corrosion attack (Figure 5). Detailed polarisation curves presented in Figure A7a,b,e further demonstrate a pronounced influence of conversion time on the electrochemical response of both TCP systems, with prolonged conversion times generally resulting in improved corrosion resistance.

Interestingly, comparison with electrochemical measurements performed shortly after deposition indicates that prolonged salt spray exposure did not lead to degradation of the optimised TCP coatings ST650 and B30002, but rather to progressive stabilisation of their protective behaviour. Similar behaviour was previously reported for TCP systems containing hydrated oxide structures and defect-containing barrier layers [72]. Li et al. [72] proposed that prolonged chloride exposure may promote the formation of additional aluminium oxide and hydroxide species within hydrated transport channels and defects, thereby increasing charge-transfer resistance and improving barrier properties. Comparable stabilisation and defect-sealing processes were described in our previous studies on zirconium-based conversion coatings deposited on various aluminium alloys exposed to chloride-containing environments [51,52,54–56], where the gradual transformation of fluoride-containing species into hydrated oxides and hydroxides has been shown to contribute to reduced coating porosity and improved barrier properties. Similar effects were additionally reported for intentionally sealed conversion coatings [73], where enhanced corrosion resistance was associated with suppression of cathodic activity and partial pore closure. Although detailed microstructural analyses were not performed for B30002 in the

present study, the combination of very low corrosion current density, high polarisation resistance and minimal visual degradation suggests that similar stabilisation processes may also occur in this system during prolonged chloride exposure.

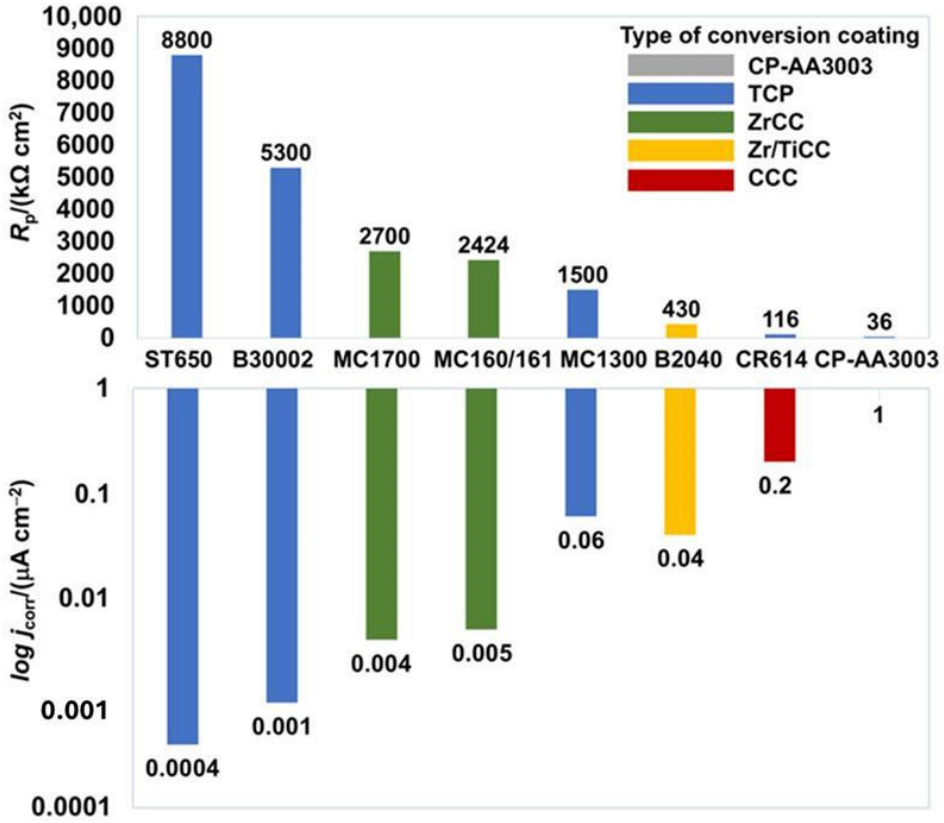

Figure 6. Comparative presentation of polarisation resistance (R_p) and corrosion current density (j_{corr}) of conversion coatings on CP-AA3003 after 500 h exposure in a salt spray chamber. The j_{corr} values are presented on a logarithmic scale.

The ZrCC systems MC1700 and MC160/161 also exhibited relatively favourable long-term electrochemical behaviour after salt spray exposure, although their protective performance remained somewhat lower than that of the optimised TCP coatings. MC1700 exhibited an R_p of around 2700 kΩ cm^2 and a j_{corr} of 0.004 μA cm^{-2}, while MC160/161 reached an R_p of around 2400 kΩ cm^2 and a j_{corr} of 0.005 μA cm^{-2} (Table 6, Figure 6). Both coatings additionally maintained visual appearance during exposure without pronounced localised corrosion attacks (Figure 5). Figure A7c,f further show a pronounced influence of conversion time on the corrosion response of both systems.

For MC1700, the coating prepared at 10 min conversion time exhibited the most favourable overall behaviour, combining high polarisation resistance, low corrosion current density and minimal visible degradation after prolonged exposure. Previous surface analyses reported in our earlier study [54] showed that the optimised MC1700 coating forms a relatively homogeneous Zr-rich conversion layer with locally intensified growth around intermetallic particles, which likely contributes to improved electrochemical stability during chloride exposure. Similar relationships between conversion conditions, intermetallic particle activity, coating homogeneity and corrosion performance of Zr conversion coatings on aluminium alloys were also reported by Kraš et al. [57]. In contrast, shorter conversion time resulted in incomplete surface coverage, whereas prolonged conversion time led to increased local heterogeneity and less stable long-term behaviour despite relatively low corrosion current densities.

The MAVOMcoat 160/161 system exhibited relatively stable behaviour during prolonged exposure without pronounced localised corrosion attacks. Interestingly, the electrochemical response after prolonged salt spray exposure differed from the behaviour observed after short-term NaCl immersion. While shorter conversion times exhibited relatively favourable behaviour after 24 h immersion in NaCl solution (Figure A6b and Table A6), longer conversion times resulted in superior long-term stability after salt spray exposure, with the 18 min coating exhibiting the highest R_p and lowest j_{corr} values (Figure A7f, Table A7). These observations demonstrate that short-term electrochemical tests alone are insufficient for reliable prediction of long-term atmospheric corrosion behaviour.

In contrast to TCP and optimised ZrCC systems, the B2040 (Zr/TiCC) coating exhibited the least favourable long-term electrochemical behaviour among the investigated chromate-free systems. The electrochemical response strongly depended on conversion time, with the shortest conversion time (80 s) exhibiting the most favourable overall behaviour after exposure (Figure A7d, Table A7). The optimised B2040 coating reached an R_p of around 430 kΩ cm^2 and a j_{corr} of 0.04 µA cm^{-2}, whereas longer conversion times resulted in substantially lower polarisation resistance and increased corrosion activity (Table A7). Visual inspection additionally revealed progressive surface degradation accompanied by the formation of corrosion products during exposure (Figure 5). The poor long-term behaviour of B2040 is consistent with the highly acidic nature of the conversion bath, which likely promotes excessive substrate dissolution during coating formation and prevents the development of a compact and stable protective layer. Interestingly, electrochemical measurements after exposure still showed a partial increase in polarisation resistance compared to the initial state. However, this apparent electrochemical improvement is more likely associated with the formation of secondary aluminium corrosion products during prolonged exposure rather than with intrinsic stabilisation of the conversion coating itself.

The conventional chromate conversion coating CR614 exhibited less favourable electrochemical behaviour than several investigated chromate-free systems after prolonged exposure. Although the coating maintained relatively high ΔE values, indicating resistance to localised breakdown processes, its polarisation resistance remained low (116 kΩ cm^2), and the corrosion current density remained substantially higher than for TCP and optimised ZrCC systems (Table 6, Figure 6). Visual inspection revealed only minor visible surface changes during exposure (Figure 5). The results therefore demonstrate that several investigated chromate-free conversion coating systems, particularly optimised TCP coatings and selected ZrCC systems, may provide corrosion protection comparable to or even superior to the investigated CCC system under prolonged chloride exposure conditions.

Overall, the results clearly demonstrate that prolonged salt spray exposure provides substantially greater differentiation between the investigated conversion coating systems than short-term electrochemical exposure tests. The long-term corrosion response strongly depends not only on coating chemistry but also on conversion time and the ability of the coating to maintain electrochemical stability during prolonged chloride exposure. The results further confirm that optimised TCP coatings exhibit the most favourable combination of long-term barrier stability and resistance to localised corrosion, while optimised ZrCC systems also provide highly promising corrosion protection on AA3003 alloy.

Although the thickness was not determined for each coating, which is a limitation of the study, previous studies [42,52,54,56] showed that the thickness of the conversion coatings is in the 50–200 nm range.

4. Conclusions

The investigated conversion coatings exhibited different electrochemical behaviour depending on the exposure conditions. After short-term exposure, differences between the investigated systems remained relatively limited, particularly in the simulated acid rain solution. In contrast, chloride-containing environments enabled clearer differentiation of coating performance, with most coatings providing improved corrosion resistance compared to the chemically pre-treated substrate.

Among the investigated systems, the TCP coatings ST650 and B30002 exhibited the most favourable overall corrosion behaviour, achieving the highest polarisation resistance and lowest corrosion current density values, particularly after 500 h salt spray exposure. The ZrCC systems MC1700 and MC160/161 also provided significant corrosion protection, whereas the Zr/TiCC coating B2040 exhibited the least favourable long-term performance.

The 500 h salt spray test revealed substantially greater differences between the investigated systems than short-term electrochemical measurements and proved more suitable for evaluating long-term coating stability.

Overall, under salt spray testing conditions, optimised TCP and ZrCC coatings provided corrosion protection comparable to or superior to the investigated conventional chromate conversion coating CR614 deposited on AA3003 alloy. A limitation of the study is that only one specific chromate system was analysed, so future studies may involve a comparison of multiple chromate-based coatings.

Author Contributions: Conceptualization, M.M.K. and I.M.; methodology, M.M.K. and I.M.; investigation, M.M.K.; electrochemical measurement, M.M.K.; formal analysis, M.M.K.; data curation, M.M.K.; writing—original draft preparation, M.M.K.; writing—review and editing, M.M.K. and I.M.; visualization, M.M.K.; supervision, I.M. All authors have read and agreed to the published version of the manuscript.

Funding: I. M. acknowledges the Slovenian Research and Innovation Agency for providing core funding (grant no. P2-0393).

Data Availability Statement: The raw data supporting the conclusions of this article will be made available by the authors on request.

Acknowledgments: During the preparation of this manuscript, the authors used ChatGPT (OpenAI, GPT-5.5) for language editing, text refinement, improvement of scientific writing and preparation of one graphical illustration. The authors reviewed and edited the generated content and take full responsibility for the content of this publication.

Conflicts of Interest: Maja Mujdrica Kim was employed by the company Trimo d.o.o. The remaining author declares that the research was conducted in the absence of any commercial or financial relationships that could be construed as a potential conflict of interest.

Abbreviations

The following abbreviations are used in this manuscript:

CCC	chromate conversion coating
CSRD	Corporate Sustainability Reporting Directive
ESPR	Ecodesign for Sustainable Products Regulation
OCP	open circuit potential
PD	potentiodynamic polarization
RT	room temperature
TCP	trivalent chromium process
ZrCC	zirconium-based conversion coating
Zr/TiCC	zirconium/titanium-based conversion coatings

Appendix A

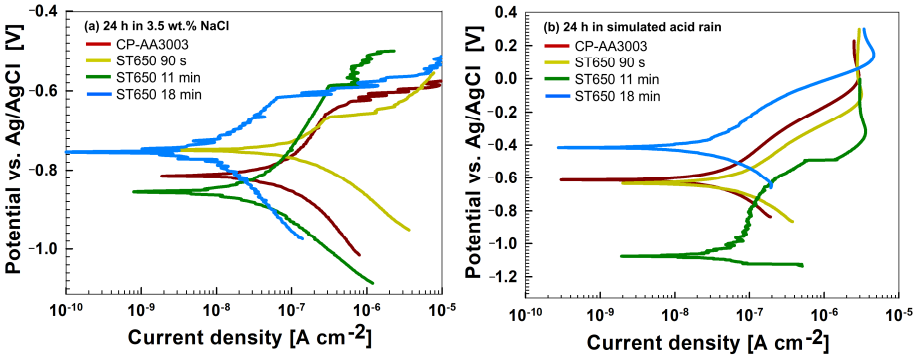

Figure A1. Potentiodynamic polarisation curves recorded for chemically pre-treated CP-AA3003 and ST650-coated samples prepared at different conversion times and exposed for 24 h to different post-treatment environments: (**a**) 3.5 wt.% NaCl solution and (**b**) simulated acid rain. Electrochemical measurements were performed in 3.5 wt.% NaCl solution for (**a**) and in simulated acid rain solution for (**b**). The scan rate was dE/dt = 1 mV/s. Electrochemical parameters deduced from the curves are presented in Table A1.

Table A1. Electrochemical parameters were deduced from potentiodynamic measurements for chemically pre-treated CP-AA3003 and ST650-coated samples prepared at different conversion times and exposed for 24 h to different post-treatment environments. The polarisation resistance (R_p) was determined from the linear polarisation measurements, and the corrosion potential (E_{corr}), corrosion current density (j_{corr}), breakdown potential (E_{bd}) and $\Delta E = |E_{bd} - E_{corr}|$ from potentiodynamic polarisation curves (Figure A1). Values are given as mean ± standard deviation. The selected optimal conversion times are written in bold.

Post-Treatment	t_{conv}	R_p (kΩ cm^2)	E_{corr} (V)	j_{corr} (μA cm^{-2})	E_{bd} (V)	ΔE (V)
24 h in 3.5 wt.% NaCl	CP-AA3003	740 ± 50	−0.80 ± 0.02	0.06 ± 0.03	−0.64 ± 0.02	0.17
	90 s	166 ± 39	−0.77 ± 0.02	0.16 ± 0.06	−0.51 ± 0.02	0.25
	11 min	1144 ± 462	−0.86 ± 0.001	0.03 ± 0.01	−0.55 ± 0.05	0.30
	18 min	1927 ± 73	−0.76 ± 0.01	0.01 ± 0.01	−0.59 ± 0.04	0.17
24 h in simulated acid rain	CP-AA3003	2000 ± 800	−0.59 ± 0.10	0.03 ± 0.01	-	-
	90 s	658 ± 195	−0.67 ± 0.04	0.04 ± 0.04	-	-
	11 min	575 ± 164	−1.04 ± 0.05	0.05 ± 0.01	−0.38 ± 0.16	0.66
	18 min	1545 ± 716	−0.66 ± 0.22	0.03 ± 0.02	-	-

Table A2. Electrochemical parameters were deduced from potentiodynamic measurements for chemically pre-treated CP-AA3003 and MC1300-coated samples prepared at different conversion times and exposed for 24 h to different post-treatment environments. The polarisation resistance (R_p) was determined from the linear polarisation measurements, and the corrosion potential (E_{corr}), corrosion current density (j_{corr}), breakdown potential (E_{bd}) and $\Delta E = |E_{bd} - E_{corr}|$ from potentiodynamic polarisation curves (Figure A2). Values are given as mean ± standard deviation. The selected optimal conversion times are written in bold.

Post-Treatment	t_{conv}	R_p (kΩ cm^2)	E_{corr} (V)	j_{corr} (μA cm^{-2})	E_{bd} (V)	ΔE (V)
24 h in air	CP-AA3003	1300 ± 200	−0.80 ± 0.01	0.02 ± 0.01	−0.68 ± 0.01	0.12
	80 s	30 ± 3	−0.74 ± 0.03	0.09 ± 0.04	−0.67 ± 0.01	0.07
	7 min	190 ± 40	−0.72 ± 0.04	0.13 ± 0.11	−0.68 ± 0.02	0.04
	18 min	62 ± 9	−0.72 ± 0.02	0.15 ± 0.04	−0.64 ± 0.01	0.09
	45 min	22 ± 2	−0.68 ± 0.02	0.82 ± 0.15	-	-

Table A2. *Cont.*

Post-Treatment	t_{conv}	R_p (kΩ cm^2)	E_{corr} (V)	j_{corr} (μA cm^{-2})	E_{bd} (V)	ΔE (V)
24 h in 3.5 wt.% NaCl	CP-AA3003	740 ± 50	−0.82 ± 0.02	0.06 ± 0.03	−0.64 ± 0.02	0.17
	80 s	2000 ± 100	−0.76 ± 0.03	0.01 ± 0.04	−0.57 ± 0.04	0.18
	7 min	890 ± 70	−0.86 ± 0.01	0.05 ± 0.01	−0.67 ± 0.01	0.18
	18 min	260 ± 90	−0.71 ± 0.02	0.05 ± 0.01	−0.64 ± 0.01	0.09
	45 min	63 ± 14	−0.72 ± 0.05	0.37 ± 0.08	−0.61 ± 0.01	0.11
24 h in simulated acid rain	CP-AA3003	830 ± 230	−0.76 ± 0.01	0.07 ± 0.02	-	-
	80 s	520 ± 260	−0.58 ± 0.16	0.08 ± 0.01	-	-
	7 min	95 ± 23	−0.46 ± 0.05	0.62 ± 0.08	-	-
	18 min	340 ± 220	−0.39 ± 0.05	0.17 ± 0.12	-	-
	45 min	28 ± 7	−0.78 ± 0.08	1.08 ± 0.23	-	-

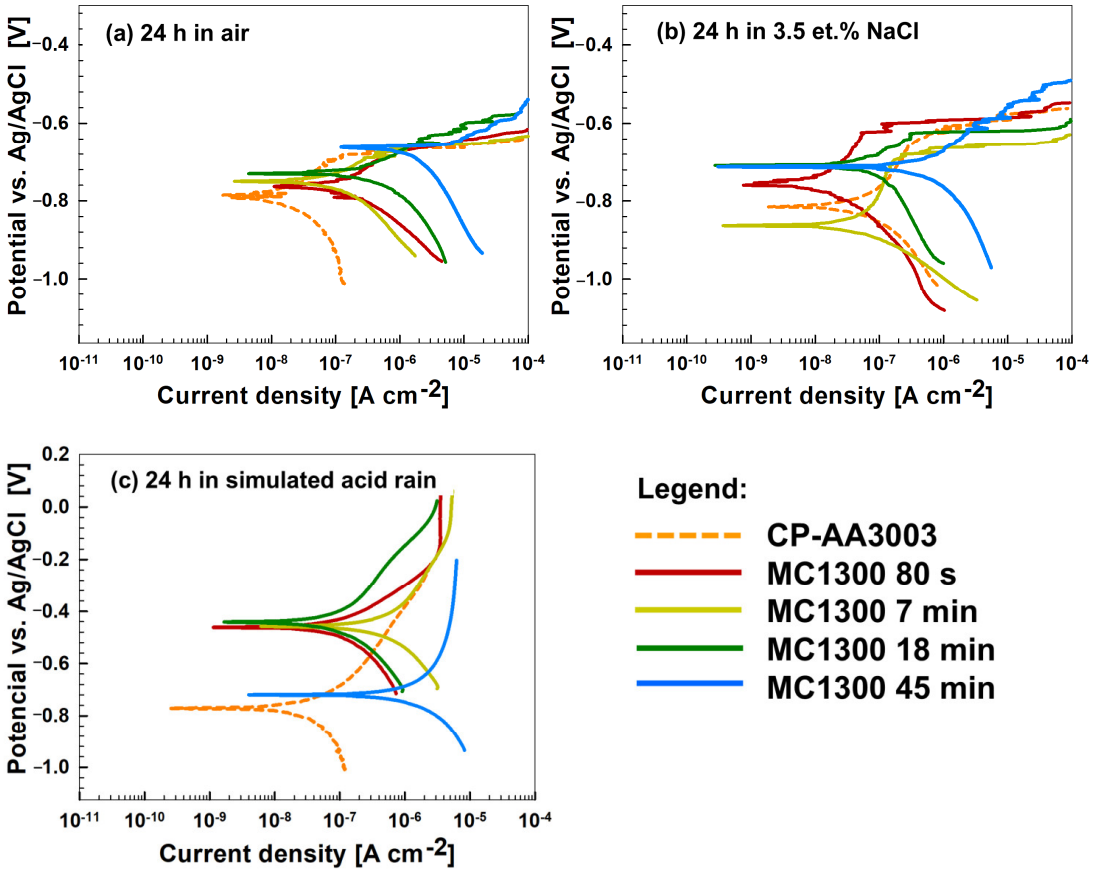

Figure A2. Potentiodynamic polarisation curves recorded for chemically pre-treated CP-AA3003 and MC1300-coated samples prepared at different conversion times and exposed for 24 h to different post-treatment environments: (**a**) 24 h in air, (**b**) 3.5 wt.% NaCl solution and (**c**) simulated acid rain. Potentiodynamic measurements for samples shown in (**a**,**b**) were performed in 3.5 wt.% NaCl solution, whereas measurements for samples shown in (**c**) were performed in simulated acid rain solution. The scan rate was dE/dt = 1 mV/s. Electrochemical parameters deduced from the curves are presented in Table A2.

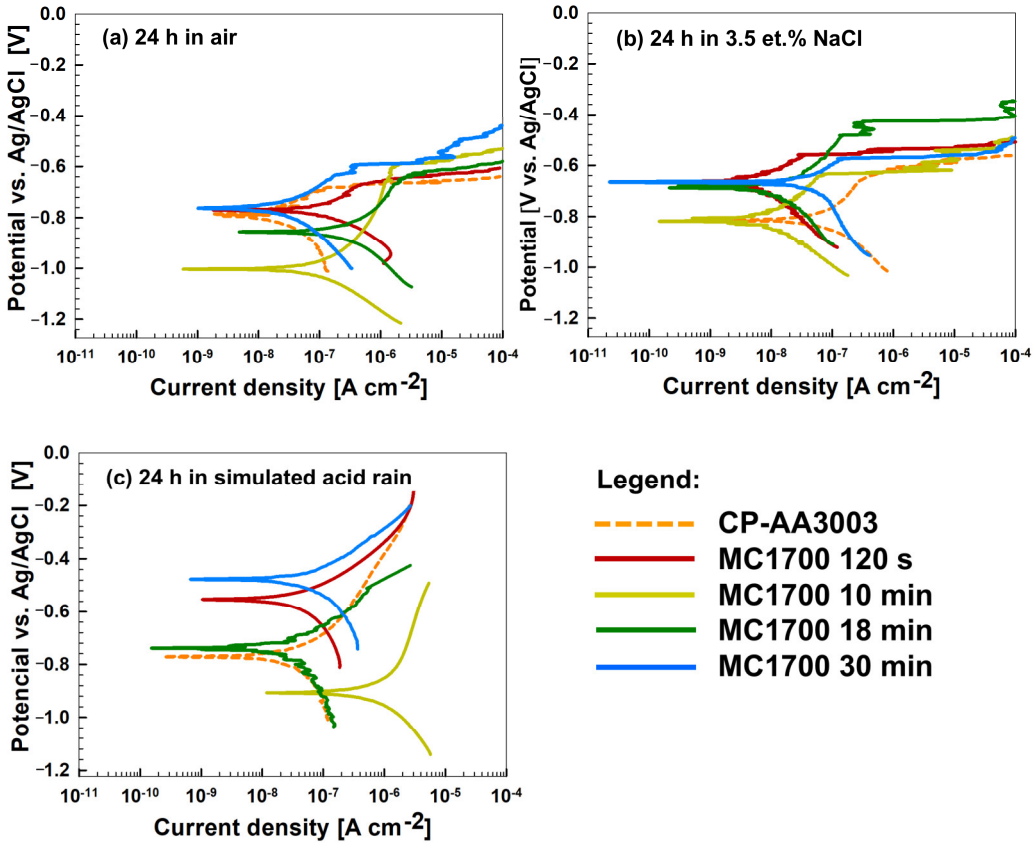

Figure A3. Potentiodynamic polarisation curves recorded for chemically pre-treated CP-AA3003 and MC1700-coated samples prepared at different conversion times and exposed for 24 h to different post-treatment environments: (**a**) 24 h in air, (**b**) 3.5 wt.% NaCl solution and (**c**) simulated acid rain. Potentiodynamic measurements for samples shown in (**a**,**b**) were performed in 3.5 wt.% NaCl solution, whereas measurements for samples shown in (**c**) were performed in simulated acid rain solution. The scan rate was dE/dt = 1 mV/s. Electrochemical parameters deduced from the curves are presented in Table A3.

Table A3. Electrochemical parameters were deduced from potentiodynamic measurements for chemically pre-treated CP-AA3003 and MC1700-coated samples prepared at different conversion times and exposed for 24 h to different post-treatment environments. The polarisation resistance (R_p) was determined from the linear polarisation measurements, and the corrosion potential (E_{corr}), corrosion current density (j_{corr}), breakdown potential (E_{bd}) and $\Delta E = |E_{bd} - E_{corr}|$ from potentiodynamic polarisation curves (Figure A3). Values are given as mean ± standard deviation. The selected optimal conversion times are written in bold.

Post-Treatment	t_{conv}	R_p (kΩ cm^2)	E_{corr} (V)	j_{corr} (μA cm^{-2})	E_{bd} (V)	ΔE (V)
24 h in air	CP-AA3003	1300 ± 200	−0.80 ± 0.01	0.02 ± 0.01	−0.68 ± 0.01	0.12
	120 s	30 ± 60	−0.79 ± 0.02	0.14 ± 0.06	−0.68 ± 0.01	0.11
	10 min	500 ± 60	−1.01 ± 0.01	0.08 ± 0.01	−0.59 ± 0.02	0.42
	18 min	170 ± 60	−0.85 ± 0.04	0.30 ± 0.02	−0.63 ± 0.01	0.23
	30 min	1000 ± 300	−0.67 ± 0.14	0.02 ± 0.01	−0.56 ± 0.04	0.1
24 h in 3.5 wt.% NaCl	CP-AA3003	730 ± 60	−0.82 ± 0.02	0.06 ± 0.03	−0.64 ± 0.02	0.17
	120 s	2700 ± 300	−0.73 ± 0.08	0.01 ± 0.02	−0.59 ± 0.04	0.14
	10 min	2000 ± 470	−0.80 ± 0.02	0.01 ± 0.03	−0.63 ± 0.01	0.17
	18 min	1700 ± 650	−0.68 ± 0.01	0.02 ± 0.01	−0.44 ± 0.01	0.24
	30 min	650 ± 100	−0.67 ± 0.01	0.05 ± 0.03	−0.57 ± 0.01	0.09

Table A3. *Cont.*

Post-Treatment	t_{conv}	R_p (kΩ cm^2)	E_{corr} (V)	j_{corr} (μA cm^{-2})	E_{bd} (V)	ΔE (V)
24 h in simulated acid rain	CP-AA3003	830 ± 230	−0.76 ± 0.01	0.07 ± 0.02	-	-
	120 s	1200 ± 320	−0.59 ± 0.05	0.05 ± 0.02	-	-
	10 min	62 ± 19	−0.91 ± 0.03	1.1 ± 0.05	-	-
	18 min	170 ± 40	−0.77 ± 0.04	0.03 ± 0.01	-	-
	30 min	650 ± 40	−0.45 ± 0.04	0.05 ± 0.01	-	-

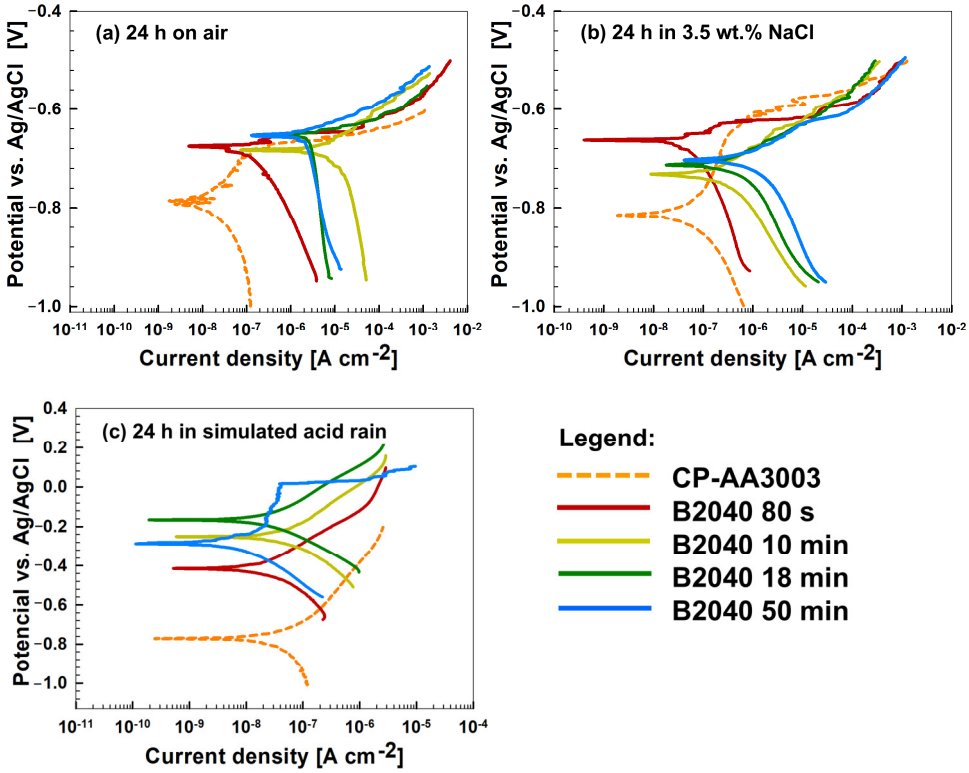

Figure A4. Potentiodynamic polarisation curves recorded for chemically pre-treated CP-AA3003 and B2040-coated samples prepared at different conversion times and exposed for 24 h to different post-treatment environments: (**a**) 24 h in air, (**b**) 3.5 wt.% NaCl solution and (**c**) simulated acid rain. Potentiodynamic measurements for samples shown in (**a**,**b**) were performed in 3.5 wt.% NaCl solution, whereas measurements for samples shown in (**c**) were performed in simulated acid rain solution. The scan rate was dE/dt = 1 mV/s. Electrochemical parameters deduced from the curves are presented in Table A4.

Table A4. Electrochemical parameters were deduced from potentiodynamic measurements for chemically pre-treated CP-AA3003 and B2040-coated samples prepared at different conversion times and exposed for 24 h to different post-treatment environments. The polarisation resistance (R_p) was determined from the linear polarisation measurements, and the corrosion potential (E_{corr}), corrosion current density (j_{corr}), breakdown potential (E_{bd}) and $\Delta E = |E_{bd} - E_{corr}|$ from potentiodynamic polarisation curves (Figure A4). Values are given as mean ± standard deviation. The selected optimal conversion times are written in bold.

Post-Treatment	t_{conv}	R_p (kΩ cm^2)	E_{corr} (V)	j_{corr} (μA cm^{-2})	E_{bd} (V)	ΔE (V)
24 h in air	CP-AA3003	1300 ± 200	−0.80 ± 0.01	0.02 ± 0.01	−0.68 ± 0.01	0.12
	80 s	14 ± 10	−0.71 ± 0.04	1 ± 2	−0.72 ± 0.04	0.01

Table A4. *Cont.*

Post-Treatment	t_{conv}	R_p (kΩ cm^2)	E_{corr} (V)	j_{corr} (μA cm^{-2})	E_{bd} (V)	ΔE (V)
24 h in air	10 min	5 ± 3	−0.67 ± 0.02	4 ± 3	−0.65 ± 0.02	0.02
	18 min	3 ± 1	−0.66 ± 0.04	2.6 ± 0.7	−0.62 ± 0.01	0.04
	50 min	7 ± 3	−0.66 ± 0.01	2.4 ± 0.2	−0.58 ± 0.02	0.08
24 h in 3.5 wt.% NaCl	CP-AA3003	740 ± 50	−0.80 ± 0.02	0.06 ± 0.03	−0.64 ± 0.02	0.17
	80 s	50 ± 30	−0.67 ± 0.01	0.10 ± 0.06	−0.63 ± 0.01	0.03
	10 min	26 ± 1	−0.71 ± 0.03	0.5 ± 0.3	−0.66 ± 0.01	0.05
	18 min	9 ± 2	−0.70 ± 0.01	0.78 ± 0.12	−0.66 ± 0.01	0.10
	50 min	10 ± 5	−0.69 ± 0.01	0.9 ± 0.2	−0.64 ± 0.01	0.02
24 h in simulated acid rain	CP-AA3003	830 ± 230	−0.76 ± 0.01	0.07 ± 0.03	-	-
	80 s	260 ± 130	−0.41 ± 0.02	0.05 ± 0.04	-	-
	10 min	620 ± 270	−0.24 ± 0.02	0.06 ± 0.03	-	-
	18 min	990 ± 570	−0.16 ± 0.01	0.03 ± 0.01	-	-
	50 min	2800 ± 1200	−0.31 ± 0.03	0.002 ± 0.001	0.24 ± 0.30	0.31

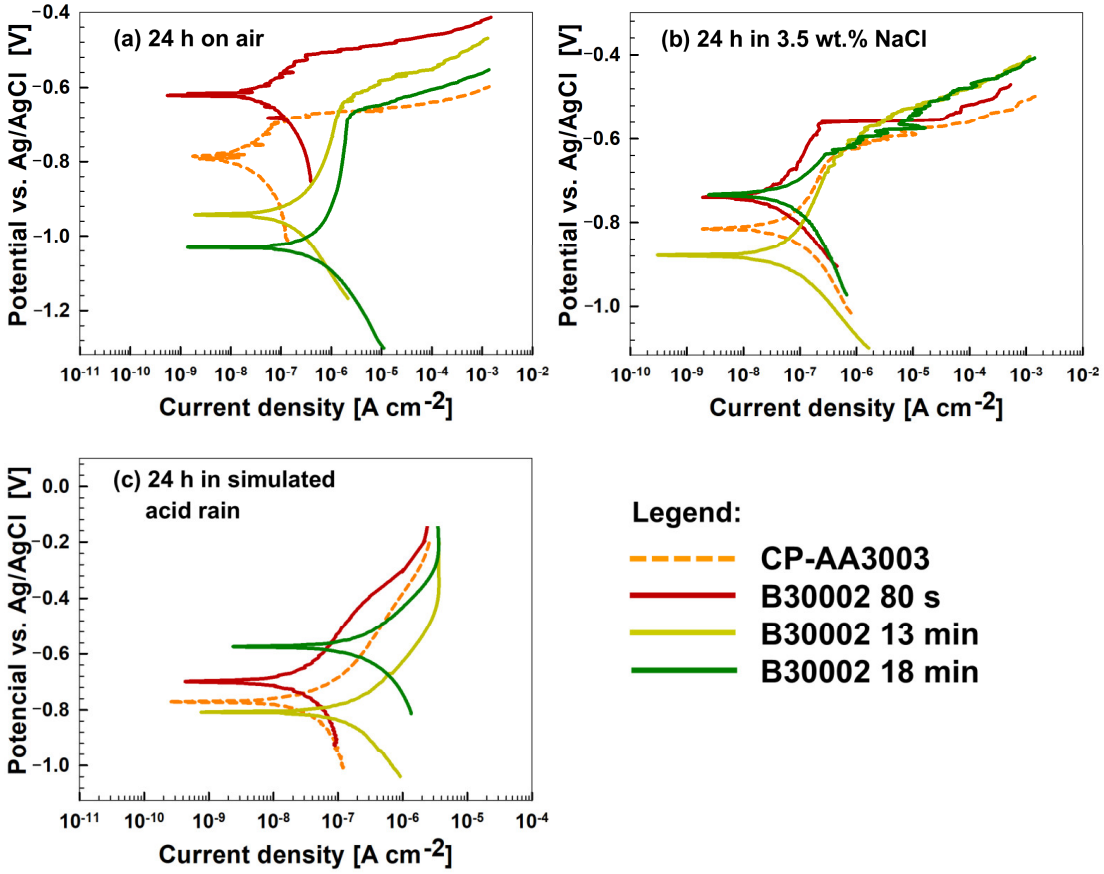

Figure A5. Potentiodynamic polarisation curves recorded for chemically pre-treated CP-AA3003 and B30002-coated samples prepared at different conversion times and exposed for 24 h to different post-treatment environments: (**a**) 24 h in air, (**b**) 3.5 wt.% NaCl solution and (**c**) simulated acid rain. Potentiodynamic measurements for samples shown in (**a**,**b**) were performed in 3.5 wt.% NaCl solution, whereas measurements for samples shown in (**c**) were performed in simulated acid rain solution. The scan rate was dE/dt = 1 mV/s. Electrochemical parameters deduced from the curves are presented in Table A5.

Table A5. Electrochemical parameters were deduced from potentiodynamic measurements for chemically pre-treated CP-AA3003 and B30002-coated samples prepared at different conversion times and exposed for 24 h to different post-treatment environments. The polarisation resistance (R_p) was determined from the linear polarisation measurements, and the corrosion potential (E_{corr}), corrosion current density (j_{corr}), breakdown potential (E_{bd}) and $\Delta E = |E_{bd} - E_{corr}|$ from potentiodynamic polarisation curves (Figure A5). Values are given as mean ± standard deviation. The selected optimal conversion times are written in bold.

Post-Treatment	t_{conv}	R_p (kΩ cm^2)	E_{corr} (V)	j_{corr} (μA cm^{-2})	E_{bd} (V)	ΔE (V)
24 h in air	CP-AA3003	1300 ± 200	−0.80 ± 0.01	0.02 ± 0.01	−0.68 ± 0.01	0.12
	80 s	610 ± 90	−0.61 ± 0.02	0.09 ± 0.02	−0.50 ± 0.04	0.11
	13 min	290 ± 3	−0.90 ± 0.06	0.18 ± 0.01	−0.63 ± 0.01	0.28
	18 min	77 ± 1	−1.01 ± 0.02	0.61 ± 0.09	−0.69 ± 0.01	0.33
24 h in 3.5 wt.% NaCl	CP-AA3003	740 ± 50	−0.82 ± 0.02	0.06 ± 0.03	−0.64 ± 0.02	0.17
	80 s	840 ± 10	−0.76 ± 0.02	0.01 ± 0.07	−0.54 ± 0.01	0.22
	13 min	730 ± 60	−0.90 ± 0.02	0.06 ± 0.01	−0.52 ± 0.01	0.38
	18 min	430 ± 30	−0.71 ± 0.04	0.06 ± 0.01	-	-
24 h in simulated acid rain	CP-AA3003	830 ± 230	−0.76 ± 0.01	0.07 ± 0.03	-	-
	80 s	880 ± 110	−0.79 ± 0.14	0.06 ± 0.05	-	-
	13 min	330 ± 90	−0.81 ± 0.05	0.19 ± 0.07	-	-
	18 min	180 ± 70	−0.58 ± 0.01	0.20 ± 0.03	-	-

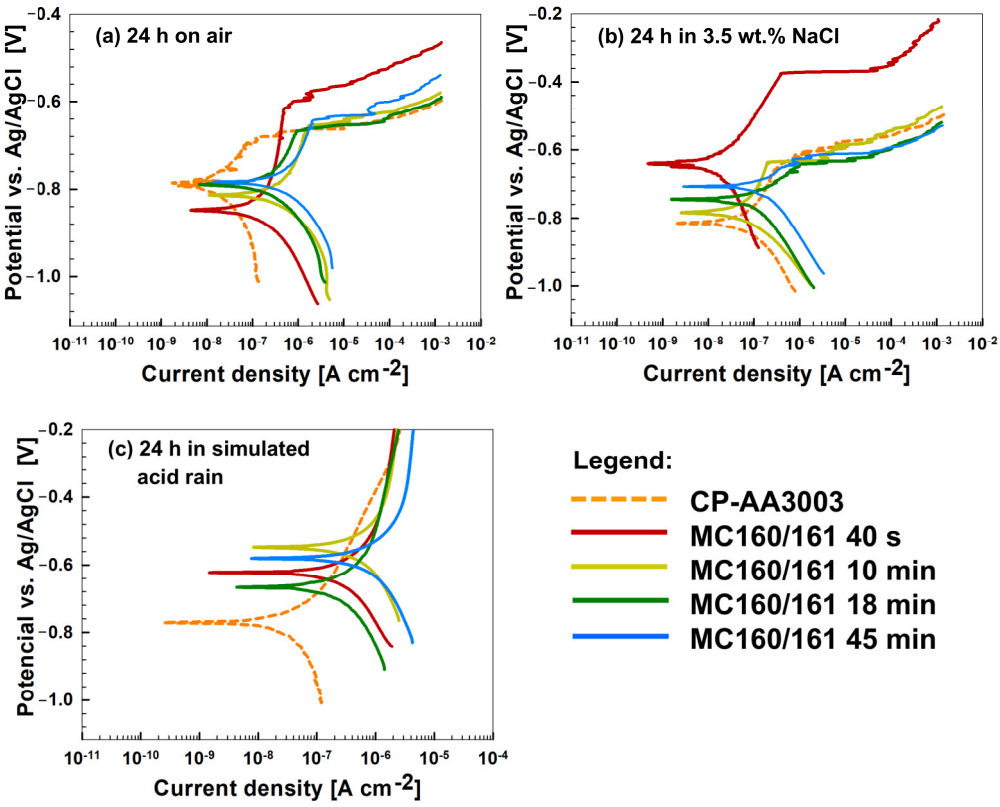

Figure A6. Potentiodynamic polarisation curves recorded for chemically pre-treated CP-AA3003 and MC160/161-coated samples prepared at different conversion times and exposed for 24 h to different post-treatment environments: (**a**) 24 h in air, (**b**) 3.5 wt.% NaCl solution and (**c**) simulated acid rain. Potentiodynamic measurements for samples shown in (**a**,**b**) were performed in 3.5 wt.% NaCl solution, whereas measurements for samples shown in (**c**) were performed in simulated acid rain solution. The scan rate was dE/dt = 1 mV/s. Electrochemical parameters deduced from the curves are presented in Table A6.

Table A6. Electrochemical parameters were deduced from potentiodynamic measurements for chemically pre-treated CP-AA3003 and MC160/161-coated samples prepared at different conversion times and exposed for 24 h to different post-treatment environments. The polarisation resistance (R_p) was determined from the linear polarisation measurements, and the corrosion potential (E_{corr}), corrosion current density (j_{corr}), breakdown potential (E_{bd}) and $\Delta E = |E_{bd} - E_{corr}|$ from potentiodynamic polarisation curves (Figure A6). Values are given as mean ± standard deviation. The selected optimal conversion times are written in bold.

Post-Treatment	t_{conv}	R_p (kΩ cm^2)	E_{corr} (V)	j_{corr} (μA cm^{-2})	E_{bd} (V)	ΔE (V)
24 h in air	CP-AA3003	735 ± 523	−0.82 ± 0.02	0.06 ± 0.03	−0.64 ± 0.02	0.17
	40 s	226 ± 81	−0.92 ± 0.11	0.21 ± 0.06	−0.64 ± 0.03	0.29
	10 min	99 ± 43	−0.79 ± 0.03	0.28 ± 0.11	−0.64 ± 0.02	0.15
	18 min	188 ± 32	−0.78 ± 0.01	0.12 ± 0.09	−0.67 ± 0.01	0.11
	45 min	66 ± 6	−0.76 ± 0.02	0.23 ± 0.08	−0.65 ± 0.01	0.11
24 h in 3.5 wt.% NaCl	CP-AA3003	740 ± 50	−0.82 ± 0.02	0.06 ± 0.03	−0.64 ± 0.02	0.17
	40 s	1500 ± 537	−0.63 ± 0.03	0.03 ± 0.02	−0.38 ± 0.01	0.25
	10 min	218 ± 321	−0.63 ± 0.04	0.12 ± 0.04	−0.61 ± 0.02	0.11
	18 min	266 ± 11	−0.75 ± 0.02	0.07 ± 0.01	−0.64 ± 0.01	0.1
	45 min	138 ± 12	−0.68 ± 0.03	0.08 ± 0.04	−0.61 ± 0.01	0.07
24 h in simulated acid rain	CP-AA3003	825 ± 229	−0.76 ± 0.01	0.06 ± 0.03	-	-
	40 s	114 ± 56	−0.62 ± 0.03	0.24 ± 0.11	-	-
	10 min	171 ± 130	−0.60 ± 0.07	0.38 ± 0.29	-	-
	18 min	286 ± 196	−0.46 ± 0.18	0.11 ± 0.16	-	-
	45 min	100 ± 21	−0.60 ± 0.03	0.46 ± 0.31	-	-

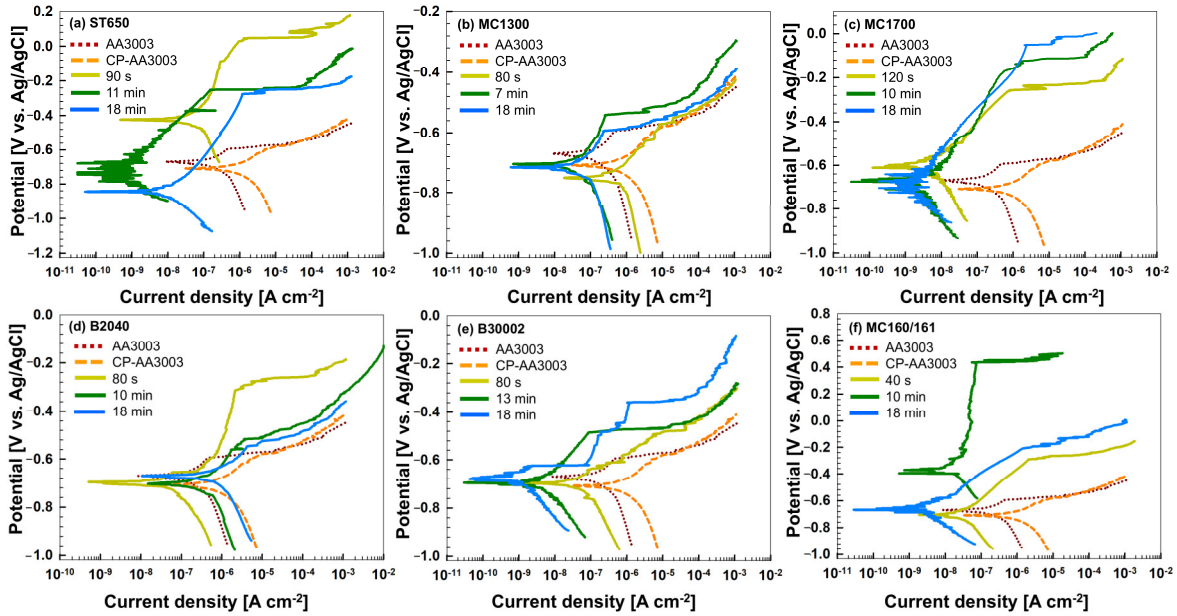

Figure A7. Potentiodynamic polarisation curves recorded for chemically pre-treated CP-AA3003 and conversion-coated samples prepared at different conversion times and exposed for 500 h in a salt spray chamber: (**a**) ST650, (**b**) MC1300, (**c**) MC1700, (**d**) B2040, (**e**) B30002 and (**f**) MC160/161. Electrochemical measurements were performed in 3.5 wt.% NaCl solution. The scan rate was $dE/dt = 1$ mV/s. Electrochemical parameters deduced from the curves are presented in Table A7.

Table A7. Electrochemical parameters were deduced from potentiodynamic measurements for chemically pre-treated CP-AA3003 and conversion-coated samples prepared at different conversion times and exposed for 500 h in a salt spray chamber. The polarisation resistance (R_p) was determined from the linear polarisation measurements, and the corrosion potential (E_{corr}), corrosion current density (j_{corr}), breakdown potential (E_{bd}) and $\Delta E = |E_{bd} - E_{corr}|$ from potentiodynamic polarisation curves (Figure A7). Values are given as mean ± standard deviation. The selected optimal conversion times are written in bold.

Sample	t_{conv}	R_p (kΩ cm^2)	E_{corr} (V)	j_{corr} (μA cm^{-2})	E_{bd} (V)	ΔE (V)
CP-AA3003	-	36 ± 3	−0.71 ± 0.01	1.00 ± 0.37	−0.59 ± 0.01	0.13
ST650	90 s	780 ± 170	−0.56 ± 0.19	0.06 ± 0.019	−0.32 ± 0.33	0.23
	11 min	8800 ± 1700	−0.64 ± 0.20	0.0004 ± 0.001	−0.24 ± 0.02	0.39
	18 min	1200 ± 400	−0.83 ± 0.02	0.01 ± 0.001	−0.39 ± 0.16	0.44
MC1300	80 s	560 ± 120	−0.75 ± 0.01	0.43 ± 0.28	−0.56 ± 0.02	0.19
	7 min	370 ± 390	−0.72 ± 0.02	0.14 ± 0.13	−0.57 ± 0.02	0.15
	18 min	1500 ± 1500	−0.68 ± 0.06	0.06 ± 0.02	−0.60 ± 0.002	0.08
MC1700	120 s	2500 ± 1300	−0.70 ± 0.13	0.004 ± 0.002	−0.34 ± 0.12	0.35
	10 min	2700 ± 50	−0.72 ± 0.01	0.004 ± 0.002	−0.44 ± 0.05	0.28
	18 min	860 ± 60	−0.70 ± 0.02	0.002 ± 0.001	−0.13 ± 0.11	0.57
B2040	**80 s**	430 ± 80	−0.67 ± 0.03	0.04 ± 0.01	−0.33 ± 0.02	0.35
	10 min	70 ± 20	−0.700 ± 0.003	0.37 ± 0.07	−0.55 ± 0.05	0.15
	18 min	60 ± 40	−0.670 ± 0.001	0.6 ± 0.3	−0.550 ± 0.001	0.12
B30002	80 s	450 ± 10	−0.69 ± 0.01	0.02 ± 0.01	−0.60 ± 0.03	0.09
	13 min	3100 ± 800	−0.70 ± 0.01	0.004 ± 0.001	−0.53 ± 0.06	0.17
	18 min	5300 ± 3100	−0.83 ± 0.20	0.001 ± 0.001	−0.44 ± 0.07	0.39
MC160/161	40 s	1444 ± 577	−0.70 ± 0.005	0.02 ± 0.02	−0.44 ± 0.21	0.26
	10 min	886 ± 632	−0.53 ± 0.19	0.02 ± 0.002	−0.08 ± 0.72	0.45
	18 min	2424 ± 789	−0.69 ± 0.01	0.005 ± 0.004	−0.21 ± 0.01	0.33

References

1. Rooy, E.L. Introduction to Aluminum and Aluminum Alloys. In *Properties and Selection: Nonferrous Alloys and Special-Purpose Materials; Chapter 1; Metal Handbook*; ASM International: Materials Park, OH, USA, 1990; Volume 2, pp. 3–14. [CrossRef]
2. Luan, B.; Le, T.; Nagata, J. An investigation on the coating of 3003 aluminum alloy. *Surf. Coat. Technol.* **2004**, *186*, 431–443. [CrossRef]
3. Milošev, I.; Koblar, A. Review of coatings used for corrosion protection of aluminium alloys. *Acta Chim. Slov.* **2026**, *73*, 11–30. [CrossRef] [PubMed]
4. Tan, Y.B.; Wang, X.M.; Ma, M.; Zhang, J.X.; Liu, W.C.; Fu, R.D.; Xiang, S. A study on microstructure and mechanical properties of AA 3003 aluminum alloy joints by underwater friction stir welding. *Mater. Charact.* **2017**, *127*, 41–52. [CrossRef]
5. *EN 573-3*; Aluminium and Aluminium Alloys—Chemical Composition and Form of Wrought Products—Part 3: Chemical Composition and Form of Products. European Committee for Standardization (CEN): Brussels, Belgium, 2019. Available online: https://standards.iteh.ai (accessed on 26 May 2026).
6. Bray, J.W. Aluminium Mill and Engineered Wrought Product. In *ASM Handbook*; ASM International: Materials Park, OH, USA, 1990; Volume 2, pp. 29–61.
7. Davis, J.R. *Alloying: Understanding the Basics*; ASM International: Materials Park, OH, USA, 2001; pp. 351–416.
8. Davis, J.R. *Corrosion of Aluminum and Aluminum Alloys*; ASM International: Materials Park, OH, USA, 1999; pp. 10–23.
9. Belov, N.A.; Eskin, D.G.; Aksenov, A.A. *Multicomponent Phase Diagrams*; Elsevier: Oxford, UK, 2005; pp. 1–46.
10. Zamin, M. The Role of Mn in the Corrosion Behavior of Al-Mn Alloys. *Corrosion* **1981**, *37*, 627–632. [CrossRef]
11. Vasudevan, A.K.; Doherty, R.D. (Eds.) *Aluminum Alloys-Contemporary Research and Applications; Treatise on Materials Science and Technology*; Academic Press, Inc.: San Diego, CA, USA, 1989; Volume 31, pp. 76–83, 137–167. Available online: https://api.pageplace.de/preview/DT0400.9780323140232_A25068395/preview-9780323140232_A25068395.pdf (accessed on 26 May 2026).

12. Alexander, D.T.L.; Greer, A.L. Solid-state intermetallic phase tranformations in 3XXX aluminium alloys. *Acta Mater.* **2002**, *50*, 2571–2583. [CrossRef]
13. Liu, Y.; Meng, G.Z.; Cheng, Y.F. Electronic structure and pitting behavior of 3003 aluminum alloy passivated under various conditions. *Electrochim. Acta* **2009**, *54*, 4155–4163. [CrossRef]
14. Milošev, I.; Frankel, G.S. Review—Conversion Coatings Based on Zirconium and/or Titanium. *J. Electrochem. Soc.* **2018**, *135*, C127–C144. [CrossRef]
15. Guo, Y.; Frankel, G.S. Characterization of trivalent chromium process coating on AA2024-T3. *Surf. Coat. Technol.* **2012**, *206*, 3895–3902. [CrossRef]
16. Iyer, A.; Willis, W.; Frueh, S.; Nickerson, W.; Fowler, A.; Barnes, J.; Hagos, J.; Escarsega, J.; Scala, J.; Siub, S.L. Characterization of NAVAIR Trivalent Chromium Process (TCP) coating and solution. *Plat. Surf. Finish* **2010**, *5*, 32–42.
17. Milošev, I. Corrosion Science and Metal Protection in Support of Sustainable Development. *Electrochem. Soc. Interface* **2026**, *35*, 43. [CrossRef]
18. Prošek, T.; Keil, P.; Popova, K. Corrosion Protection and Sustainability: Why Are the Two Concepts Inherently Intertwined. *Corros. Mater. Degrad.* **2025**, *6*, 38. [CrossRef]
19. Iannuzzi, M.; Frankel, G.S. The carbon footprint of steel corrosion. *npj Mater. Degrad.* **2022**, *6*, 101. [CrossRef] [PubMed]
20. Atkins, C.; Lambert, P. Sustainability and Corrosion. *Proc. Inst. Civ. Eng. Eng. Sustain.* **2022**, *175*, 22–29. [CrossRef]
21. Regulation (EU) 2024/1781 of the European Parliament and of the Council of 13 June 2024 Establishing a Framework for the Setting of Ecodesign Requirements for Sustainable Products, Amending Directive (EU) 2020/1828 and Regulation (EU) 2023/1542 and Repealing Directive 2009/125/EC. Available online: https://eur-lex.europa.eu/eli/reg/2024/1781/oj/eng (accessed on 21 May 2026).
22. Directive (EU) 2022/2464 of the European Parliament and of the Council of 14 December 2022 Amending Regulation (EU) No 537/2014, Directive 2004/109/EC, Directive 2006/43/EC and Directive 2013/34/EU, as Regards Corporate Sustainability Reporting. Available online: https://eur-lex.europa.eu/legal-content/EN/TXT/?uri=CELEX:32022L2464 (accessed on 21 May 2026).
23. Liu, X.; Vonk, D.; Jiang, H. Environmentally Friendly Zr-Based Conversion Nanocoatings for Corrosion Inhibition of Metal Surfaces Evaluated by Multimodal X-ray Analysis. *ACS Appl. Nano Mater.* **2019**, *2*, 1920–1929. [CrossRef]
24. Mitton, D.B.; Carangelo, A.; Acquesta, A.; Monetta, T.; Curioni, M.; Bellucci, F. Selected Cr(VI) replacement options for aluminum alloys: A literature survey. *Corros. Rev.* **2017**, *35*, 365–381. [CrossRef]
25. Smit, M.A.; Sykes, J.M.; Hunter, J.A.; Sharman, J.D.B.; Scamans, G.M. Titanium based conversion coatings on aluminium alloy 3003. *Surf. Eng.* **2005**, *15*, 407–410. [CrossRef]
26. Qi, J.T.; Hashimoto, T.; Walton, J.R.; Zhou, X.; Skeldon, P.; Thompson, G.E. Trivalent chromium conversion coating formation on aluminium. *Surf. Coat. Technol.* **2015**, *280*, 317–329. [CrossRef]
27. Li, L.; Doran, K.P.; Swain, G.M. Electrochemical Characterization of Trivalent Chromium Process (TCP) Coatings on Aluminum Alloys 6061 and 7075. *J. Electrochem. Soc.* **2013**, *160*, C396–C401. [CrossRef]
28. Kraš, A.; Milošev, I. The Aqueous Chemistry of Zirconium as a Basis for Better Understanding the Formation of Zirconium Conversion Coatings: Updated Thermodynamic Data. *J. Electrochem. Soc.* **2023**, *170*, 021508. [CrossRef]
29. Samaei, A.; Chaudhuri, S. Role of zirconium conversion coating in corrosion performance of aluminum alloys: An integrated first-principles and multiphysics modeling approach. *Electrochim. Acta* **2022**, *433*, 141195. [CrossRef]
30. Sun, W.; Bian, G.; Jia, L.; Pai, J.; Ye, Z.; Wang, N.; Qi, J.; Li, T. Study of trivalent chromium conversion coating formation at solution–metal interface. *Metals* **2023**, *1*, 93. [CrossRef]
31. Liu, Y.; Yang, Y.; Zhang, C.; Zhang, T. Protection of AA5083 by a Zirconium-Based Conversion Coating. *J. Electrochem. Soc.* **2016**, *163*, C576–C586. [CrossRef]
32. Li, L.; Swain, G.P.; Howell, A.; Woodbury, D.; Swain, G.M. The Formation, Structure, Electrochemical Properties and Stability of Trivalent Chrome Process (TCP) Coatings on AA2024. *J. Electrochem. Soc.* **2011**, *158*, C274–C283. [CrossRef]
33. Li, M.; Ma, Y.; Zhang, S.; Wei, X.; Ma, M.; Wu, L.; Cui, Z.; Wu, H. Effect of Alloying Elements on the Structure and Corrosion Resistance of TCP Conversion Coating Formed on Different Aluminum Alloys. *Surf. Sci. Technol.* **2025**, *3*, 28. [CrossRef]
34. Wu, Y.-T.; Chen, S.-Y.; Yang, Z.-S.; Huang, H.-S.; Cheng, I.-C.; Lin, C.-S. Formation mechanism of Zr-based conversion coating on 6061-T6 Al and C1100 Cu galvanic couple. *Corros. Sci.* **2025**, *256*, 113188. [CrossRef]
35. León, J.; Ter-Ovanessian, B.; Normand, B.; Terryn, H.; Özkaya, B.; Lekka, M.; Grande, H.-J.; García-Lecina, E.; Vega, J.M. Corrosion resistance of electroplated coatings based on chromium trivalent-baths. *Surf. Coat. Technol.* **2024**, *481*, 130616. [CrossRef]
36. Bin Mohamad Sultan, B.; Persson, D.; Thierry, D.; Han, J.; Ogle, K. On the dissolution kinetics during acid pickling and Zr-based conversion coating of aluminum alloys using element-resolved electrochemistry. *Electrochim. Acta* **2024**, *503*, 144820. [CrossRef]
37. Qian, X.; Huang, F.; Teng, X.; Wang, Y.; Fang, Y.; Pan, J.; Wang, W.; Li, Y.; Zhan, W. The Preparation, Corrosion Resistance and Formation Mechanism of a New-Type Mo-Based Composite Conversion Coating on 6061 Aluminum Alloy. *Metals* **2023**, *13*, 168. [CrossRef]

38. Spuller, M.; Kovač, N.; Rodič, P.; Major, L.; Chwatal, S.; Cabrioli, M.; Vanazzi, M.; De Pasquale, G.; Lackner, J.M.; Kaindl, R.; et al. Cerium-containing hexamethyldisiloxane coatings for corrosion protection of a laser-based powder bed fusion fabricated AlSi10Mg0.3 alloy. *Surf. Coat. Technol.* **2025**, *506*, 132094. [CrossRef]
39. Qi, J.; Hashimoto, T.; Walton, J.; Zhou, X.; Skeldon, P.; Thompson, G.E. Formation of a Trivalent Chromium Conversion Coating on AA2024-T351 Alloy. *J. Electrochem. Soc.* **2016**, *163*, C25–C35. [CrossRef]
40. Li, L.; Kim, D.Y.; Swain, G.M. Transient Formation of Chromate in Trivalent Chromium Process (TCP) Coatings on AA2024 as Probed by Raman Spectroscopy. *J. Electrochem. Soc.* **2012**, *159*, C326–C333. [CrossRef]
41. Cai, C.; Liu, X.-Q.; Tan, X.; Li, G.-D.; Wang, H.; Li, J.-M.; Li, J.-F. A Zr- and Cr(III)-containing conversion coating on Al alloy 2024-T3 and its self-repairing behavior. *Mater. Corros.* **2016**, *68*, 338–346. [CrossRef]
42. Rodič, P.; Kapun, B.; Milošev, I. Complementary corrosion protection of cast AlSi7Mg0.3 alloy using Zr-Cr conversion and polyacrylic/siloxane-silica multilayer coatings. *npj Mater. Degrad.* **2024**, *8*, 58. [CrossRef]
43. Droniou, P.; Fristad, W.E.; Linag, J.L. Nanoceramic-based conversion coating: Ecological and economic benefits position process as a viable alternative to phosphating systems. *Met. Finish.* **2025**, *103*, 41–43. [CrossRef]
44. Xia, X.; Zhitomirsky, I.; McDermid, J.R. Electrodeposition of zinc and composite zinc–yttria stabilised zirconia coatings. *J. Mater. Process. Technol.* **2009**, *209*, 2632–2640. [CrossRef]
45. Moore, R.; Dunham, B. Zirconization™: The future of coating pretreatment processes: Alternative, phosphate-free, eco-friendly pretreatment procedure addresses energy and chemical consumption while improving product quality. *Met. Finish.* **2008**, *106*, 46–55. [CrossRef]
46. Dunham, B. Zirconium Pretreatments: Not Just for Early Adopters Anymore. *Met. Finish.* **2012**, *110*, 18–21. [CrossRef]
47. Chen, W.-K.; Bai, C.-Y.; Liu, C.-M.; Lin, C.-S.; Ger, M.-D. The effect of chromic sulfate concentration and immersion time on the structures and anticorrosive performance of the Cr(III) conversion coatings on aluminum alloys. *Appl. Surf. Sci.* **2010**, *256*, 4924–4929. [CrossRef]
48. Chen, W.K.; Lee, J.L.; Bai, C.Y.; Hou, K.H.; Ger, M.D. Growth and characteristics of Cr(III)-based conversion coating on aluminum alloy. *J. Taiwan Inst. Chem. Eng.* **2012**, *43*, 989–995. [CrossRef]
49. Zhao, J.; Hu, S.; Yu, D.; Zhu, Y.; Liu, Y.; Li, W. Performance Study on Trivalent Chromium Conversion Coatings on Surface of Aluminum-Based Reticulated Shell Structure for Large Sports Stadium. *Cailiao Baohu* **2022**, *55*, 105–108. [CrossRef]
50. Banczek, E.P.; Moraes, S.R.; Assis, S.L.; Costa, I.; Motheo, A.J. Effect of surface treatments based on self-assembling molecules and cerium coatings on the AA3003 alloy corrosion resistance. *Mater. Corros.* **2013**, *64*, 199–206. [CrossRef]
51. Šekularac, G.; Milošev, I. Electrochemical Behavior and Self-Sealing Ability of Zirconium Conversion Coating Applied on Aluminum Alloy 3005 in 0.5 M NaCl solution. *J. Electrochem. Soc.* **2020**, *167*, 021509. [CrossRef]
52. Mujdrica Kim, M.; Kapun, B.; Tiringer, U.; Šekularac, G.; Milošev, I. Protection of Aluminum Alloy 3003 in Sodium Chloride and Simulated Acid Rain Solutions by Commercial Conversion Coatings Containing Zr and Cr. *Coatings* **2019**, *9*, 563. [CrossRef]
53. Šekularac, G.; Kovač, J.; Milošev, I. Influence of Surface Pretreatments on Composition, Structure and Corrosion Performance of Zirconium Conversion Coating Applied to AA7075-T6. *J. Electrochem. Soc.* **2025**, *172*, 111501. [CrossRef]
54. Mujdrica Kim, M.; Kapun, B.; Milošev, I. Zr and Zr-Cr Commercial Conversion Coatings Deposited on 3003 Aluminium Alloy Foil. *J. Electrochem. Soc.* **2025**, *172*, 061501. [CrossRef]
55. Šekularac, G.; Kovač, J.; Milošev, I. Prolonged protection, by zirconium conversion coatings, of $AlSi_7Mg_{0.3}$ aluminium alloy in chloride solution. *Corros. Sci.* **2020**, *169*, 108615. [CrossRef]
56. Šekularac, G.; Kovač, J.; Milošev, I. Comparison of the Electrochemical Behaviour and Self-sealing of Zirconium Conversion Coatings Applied on Aluminium Alloys of series 1xxx to 7xxx. *J. Electrochem. Soc.* **2020**, *167*, 111506. [CrossRef]
57. Kraš, A.; Kramar, D.; Milošev, I. Experimental approach and assessment of Zr conversion coatings on Al alloy using response surface methodology. *Corros. Sci.* **2025**, *249*, 112824. [CrossRef]
58. Kraš, A.; Kramar, D.; Milošev, I. Characterisation of the deposition and protection performance of Zr conversion coatings on steel and zinc substrates using the response surface methodology. *Corros. Sci.* **2025**, *242*, 112551. [CrossRef]
59. Mavom Chemie BV. *MAVOMcoat 1300. Technical Data Sheet; Revision No. 01*; Mavom Chemie BV: Alphen aan den Rijn, The Netherlands, 10 July 2024.
60. Mavom Chemie BV. *MAVOMcoat 160/161. Technische gebruiksbeschrijving [Technical User Guide]; Revision No. 01*; Mavom Chemie BV: Alphen aan den Rijn, The Netherlands, 24 January 2025.
61. mavom bv. *MAVOMcoat 1700. Technische Beschrijving [Technical Description]*; mavom bv: Alphen aan den Rijn, The Netherlands, 29 September 2010.
62. SurTec Deutschland GmbH. *SurTec® 650 C chromitAL® TCP*; SurTec Deutschland GmbH: Zwingenberg, Germany, 30 January 2014.
63. Henkel Corporation. *BONDERITE M-NT 30002. Fiche Technique [Technical Data Sheet]*; Henkel Corporation: Düsseldorf, Germany, April 2014.
64. Henkel Corporation. Technical Data Sheet BONDERITE M-NT 2040. May 2022. Available online: https://datasheets.tdx.henkel.com/BONDERITE-M-NT-2040-en_GL.pdf (accessed on 27 June 2026).

65. Condoril Chemical S.r.l. *Cromcoat CR 614. Chromating Process for Aluminium and its Alloys*; Document No. LAB.CON.TC183.ST; Rev. 0; Condoroil Chemical S.r.l.: Casale Litta, Italy, April 2018.
66. Kelly, R.G. Electrochemical Thermodynamics and Kinetics of Relevance to Corrosion. In *Electrochemical Techniques in Corrosion Science and Engineering*; Kelly, R.G., Scully, J.R., Shoesmith, D., Buchheit, R.G., Eds.; Chapter 2; Marcel Dekker, Inc.: New York, NY, USA, 2003; pp. 8–53. [CrossRef]
67. *ISO 9227:2017*; Corrosion Tests in Artificial Atmospheres. Salt Spray Tests; International Organization for Standardization (ISO): Geneva, Switzerland, 2017.
68. Frankel, G.S. Pitting Corrosion of Metals: A Review of the Critical Factors. *J. Electrochem. Soc.* **1998**, *145*, 2186. [CrossRef]
69. Szklarska-Smialowska, Z. Pitting corrosion of aluminum. *Corros. Sci.* **1999**, *41*, 1743–1767. [CrossRef]
70. Li, M.; Seyeux, A.; Wiame, F.; Marcus, P.; Swiatowska, J. Insights on the Al-Cu-Fe-Mn intermetallic particles induced pitting corrosion of Al-Cu-Li alloy. *Corros. Sci.* **2020**, *176*, 109040. [CrossRef]
71. Frankel, G.S.; Buchheit, R.G.; Jaworowski, M.; Swain, G. Final Report. Scientific Understanding of Non-Chromated Corrosion Inhibitors Function. SERDP Project WP-1620. January 2013. Available online: https://apps.dtic.mil/sti/tr/pdf/ADA582500.pdf (accessed on 21 May 2026).
72. Li, L.; Swain, G.M. Effects of Aging Temperature and Time on the Corrosion Protection Provided by Trivalent Chromium Process Coatings on AA2024-T3. *ACS Appl. Mater. Interfaces* **2013**, *5*, 7923–7930. [CrossRef] [PubMed]
73. Stoica, A.I.; Światowska, J.; Romaine, A.; Di Franco, F.; Qi, J.; Mercier, D.; Seyeux, A.; Zanna, S.; Marcus, P. Influence of post-treatment time of trivalent chromium protection coating on aluminium alloy 2024-T3 on improved corrosion resistance. *Surf. Coat. Technol.* **2019**, *369*, 186–197. [CrossRef]